Vacuum 183 (2021) 109884

Contents lists available at ScienceDirect

Vacuum

journal homepage: http://www.elsevier.com/locate/vacuum

Development of a design for an ionisation vacuum gauge suitable as a reference standard

Berthold Jenninger [a,*], Johan Anderson [b], Matthias Bernien [c], Nenad Bundaleski [d], Hristiyana Dimitrova [a], Mihail Granovskij [e], Claus Illgen [c], Janez Setina [f], Karl Jousten [c], Pawel Kucharski [a], Christian Reinhardt [e], Francesco Scuderi [g], Ricardo A.S. Silva [d], Anke Stöltzel [a], Orlando M.N.D. Teodoro [d], Beata Trzpil-Jurgielewicz [a], Martin Wüest [g]

[a] CERN European Organization for Nuclear Research, 1211, Geneva 23, Switzerland
[b] RISE Research Institutes of Sweden AB, Brinellgatan 4, BOX 857, SE-501 15, Borås, Sweden
[c] Physikalisch-Technische Bundesanstalt (PTB), Abbestr. 2-12, 10587, Berlin, Germany
[d] CEFITEC, Department of Physics, Faculty of Sciences and Technology, Nova University of Lisbon, 2829-515, Caparica, Portugal
[e] VACOM Vakuum Komponenten & Messtechnik GmbH, In Den Brückenäckern, 307751, Großlöbichau, Germany
[f] IMT Institute of Metals and Technology, Lepi Pot 111000, Ljubljana, Slovenia
[g] INFICON AG, Alte Landstrasse 6LI-9496, Balzers, Liechtenstein

ARTICLE INFO

Keywords:
Ionisation gauge
Hot cathode
Sensitivity
Simulation
Reference standard

ABSTRACT

The EURAMET EMPIR project "16NRM05 - Ion gauge" aims to develop an ionisation vacuum gauge suitable as a reference vacuum standard. In such a gauge the electron trajectories and their kinetic energy inside the ionisation volume should be well defined and stable. In the search for a suitable design, a series of simulations on different ionisation gauge concepts that have the potential to meet stringent stability requirements have been carried out. Different software packages were used for this purpose. This paper focuses on the design aspects and the performance of the different ionisation gauge concepts that have been investigated by simulation. Parameters such as ionisation gauge sensitivity, ion collection efficiency and electron transmission efficiency, have been determined as a function of emission current, pressure and electron source alignment.

1. Introduction

Ionisation vacuum gauges are the most commonly used type of pressure measurement devices in high and ultrahigh vacuum. Their operation is based on the measurement of ion current produced by electron-impact ionisation of gas, which should be directly proportional to the pressure. The main parameter of any emitting cathode ionisation vacuum gauge is its sensitivity S defined as the ratio of the measured ion current at the ion collector divided by the electron emission current I_e and pressure p (ISO 27894):

$$S = \frac{I_c - I_{c0}}{I_e(p - p_0)} \quad (1)$$

I_c is the collector current at pressure p and I_{c0} the collector current at residual pressure p_0. There are many publications dealing with ionisation vacuum gauges. We carried out a systematic literature review on hot cathode ionisation gauges, with particular attention to stability issues. The outcome of this review is reported in our recent paper [1]. In summary, the measurement uncertainty of the gauges (95% confidence) on the market is 4% at best and between 10% and 20% typically [2–4], which is caused by several factors. Electron trajectories inside the ionisation volume may vary with time due to changes of electrode alignments or the emission distribution from the emitter. Surface effects such as electron stimulated desorption, X-ray emission from the grid, ion induced secondary electron emission from the ion collector, or surface poisoning of the electron emitters alter the sensitivity of a gauge with time.

The calibration and characterisation of vacuum instruments such as residual gas analysers, the measurements of pumping speed of high vacuum pumps as well as processes in industry rely on accurate measurements with ionisation vacuum gauges. In particular, for many applications there is a need of knowledge of relative gas sensitivity factors,

* Corresponding author.
E-mail address: berthold.jenninger@cern.ch (B. Jenninger).

https://doi.org/10.1016/j.vacuum.2020.109884
Received 24 August 2020; Received in revised form 22 October 2020; Accepted 28 October 2020
Available online 3 November 2020

which vary from one type of gauge to another, but also with each individual gauge. Ionisation vacuum gauges are typically calibrated for nitrogen gas only, because it would be too expensive to calibrate for several gas species. Therefore, it would be a great advantage to have a reference ionisation gauge, where relative gas sensitivity factors are accurately known from previous measurements or, even better, predictable. Such a gauge should also have a better reproducibility than those currently available.

The objective of the EURAMET EMPIR project "16NRM05 - Ion gauge" is the development of a recommended standard design for an ionisation vacuum gauge, that allows a long-term stability of 1% in the range between 10^{-6} Pa to 10^{-2} Pa. Well-defined electron trajectories and a high collection efficiency of all generated ions inside the ionisation volume will facilitate reproducible relative gas sensitivity factors. These characteristics are not achieved with the present ionisation gauges on the market. The project includes the design and manufacturing of gauges to demonstrate the validity of the recommendations.

For an ideal gauge with well-defined electron paths of length L through an ionisation volume and constant electron energy E inside that volume, the sensitivity of an ionisation gauge is given as:

$$S_{\text{ideal}} = \frac{\sigma \, L c_{ion,C}}{kT} \tag{2}$$

with σ being the electron-impact ionisation cross-section of the respective gas species at energy E (Fig. 1), $c_{ion,C}$ the ion collection efficiency (the ratio of the number of collected to produced ions inside the ionisation volume), T the absolute gas temperature inside the ionisation volume and k the Boltzmann constant. Equation (2) is valid for low gas densities with long mean free paths, where cross-section of molecules are not overlapping along the electron trajectories.

With our design proposal for a reference ionisation gauge, we try to approach the conditions of an ideal gauge aiming at predictable sensitivity and predictable relative gas sensitivity factors. In that respect, all emitted electrons should be collected by an electrode, a so-called Faraday cup. Secondary electrons and ions that are generated inside this Faraday cup should be prevented from re-entering the ionisation volume. This provides a measure of the electron emission quality, by comparing the emission current measured at the emitter and the current measured at the Faraday cup. It is essential that all emitted electrons reach the Faraday cup, i.e. that the electron transmission efficiency $\varepsilon_{et} \approx 1$, defined as ratio between the number of collected and emitted electrons. With ε_{et} and $c_{ion,C}$ both approaching 1, at a given temperature, the sensitivity for a given gas species depends only on the electron path L and the electron energy dependent ionisation cross-section of the gas molecules inside the ionisation chamber. If the electron energy is virtually constant, the sensitivity can be calculated using (2) and directly compared with measurements.

The alignment tolerances of the gauge must be sufficiently large to secure that replacements of components do not affect the gauge sensitivity. Under these conditions, no re-calibration should be required after any intervention on the gauge (e.g. replacement of an emitter).

In this paper, we explore by means of numerical simulations several designs that may be suitable as ionisation gauge reference standard. Different software packages were used for that purpose. The paper focuses on the design aspects and the performance of different ionisation gauge concepts that have been investigated by simulations, rather than comparing the simulation software themselves. Parameters such as ionisation gauge sensitivity, ion collection efficiency and electron transmission efficiency, have been determined as a function of emission current, pressure and electron source alignment.

Three programs, OPERA, SIMION and COMSOL were used. Finally, the most promising design was chosen and optimised, and the corresponding device was manufactured. The first experimental results agree

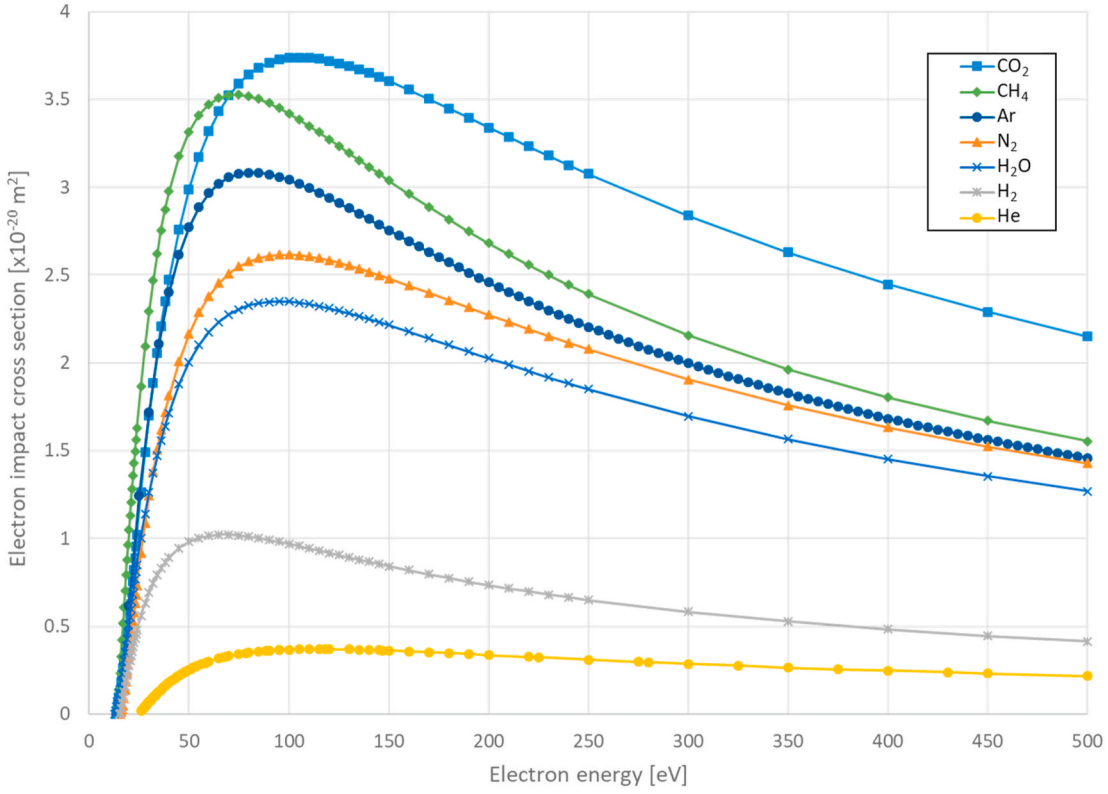

Fig. 1. Electron-impact ionisation cross-section for some common gases. Except for argon, these graphs have been calculated using the Binary-Encounter-Bethe (BEB) model following the description and data that can be found at NIST [5]. The NIST database does not provide the ionisation cross-section for argon. The graph for argon has been determined using the BEB with relativistic core potentials RECP wave functions with scaling (1.07) to fit best the available experimental data used in [6].

very well with the predictions of the simulations.

2. Requirements and considerations for a suitable design

Various ionisation gauge concepts that could meet a set of demanding requirements are explored. The most important demands are to provide well-defined electron paths through the ionisation volume, high ion collection efficiency $\varepsilon_{ic} \approx 1$, and electron transmission efficiency $\varepsilon_{et} \approx 1$, which shall not be affected by small mechanical misalignments or fluctuations of electrode potentials. However, there is a set of additional conditions that must be considered.

2.1. Ion current at lowest operation pressure

Good commercial electrometers are able to detect electrical currents down to the low femtoampere range. In order to measure ion currents with the required precision of better than 1%, a promising design should therefore provide ion currents well above this limit in the picoampere range. We aim for ion currents higher than 10 pA even at the lower operation pressure range of 10^{-6} Pa.

2.2. Preserving linearity at high pressures

A perfect linearity or constant sensitivity with pressure greatly reduces the effort of calibration and also increases the reliability of measurements. Securing a pressure-independent sensitivity in the 10^{-6} Pa to10^{-2} Pa range implies a design in which ion-induced space charge effects do not affect the pressure reading even at high pressures. One of the most critical points in that respect is the shape of the ion collector (e.g. a narrow wire as in Bayard-Alpert configuration or a plate as another extreme), since high ion density in the vicinity of the collector at higher operating pressures may perturb the electric field and thus affect the electron and ion trajectories.

2.3. Linearity with electron emission current

It would be desirable that the sensitivity is constant with electron emission current. At high emission current the sensitivity is affected by a modification of the electron trajectories caused by the mutual repelling of the negatively charged electrons. At the maximum emission current the reference gauge must fulfil the criteria of section 2.1 with respect to the minimum ion current at lowest operation pressure. A user might, however, prefer to operate the gauge at lower emission current. A constant sensitivity with emission current therefore reduces the effort of calibration.

2.4. Potential drop in heating element of thermionic emitters

In ionisation vacuum gauges with hot cathodes, the free electrons are in general produced by thermionic emission. If the emitter is a heated filament, the potential drop along the filament will cause variations of the acceleration voltage between the filament (cathode) and anode. The resulting energy spread must not influence the electron trajectories or the gauge sensitivity.

2.5. Non-uniformity of electron emission

The electron emitting surface interacts with the residual gas and is altered by ion bombardment or evaporation of material during long-term operation. This may result in changes in the local work function and/or temperature, which then affects the spatial distribution of emitted electrons. A promising design must be insensitive to such changes. We approach this challenge by reducing the emission area on the emitter, which in turn leads to an increased emission current density. By means of simulations, we then check whether emission is still possible or limited by the electron space-charge and whether electron trajectories are modified. The Richardson's law describes the electron emission from a hot surface, thermionic emission [7,8]. Using Richardson's equation (3), we can estimate the change of the absolute temperature T from the work-function W_f and the change in emission current density J of the emitter material. λ is a material-specific correlation factor (typically around 0.5) and A_0 Richardson's constant ($A_0 = 1.202\ 10^6$ A m^{-2} K^{-2}).

$$J = \lambda\, A_0 T^2 e^{\frac{-W_f}{kT}} \tag{3}$$

2.6. Secondary electrons, ions and photons

A Faraday cup is used to control the stability of the emitted electron beam. In combination with a deflector, we also isolate the ionisation volume from the area where the electrons impinge on the surface at the end of their trajectories. Secondary electrons, ions and photons produced by the impingement can therefore be prevented from entering the ionisation volume generating secondary effects. The latter will suppress e.g. X-ray induced secondary electron emission from the collector, which is a cause of non-linearity at low pressures.

2.7. Depletion of neutral molecules inside electron beam

In a design with electron beams, gas molecules will be transformed into ions within the beam and extracted from the beam volume (Fig. 2). This may cause a density (pressure) gradient between the ionisation volume and the beam volume, and therefore introduce a systematic error in the pressure measurement. In the following we will estimate the size of this effect.

The loss of neutral particles in a homogenous electron beam cylinder per time can be estimated by:

$$\frac{I^+}{e} = \frac{I_e}{e} n_b \sigma L \tag{4}$$

with e being the elementary charge. The net supply of neutrals into the beam cylinder per time is:

$$N_{supply} = (n_0 - n_b) A \bar{c} \,/\, 4 \tag{5}$$

where $\bar{c}$ is the mean velocity of the neutrals, and A is the area through which particles can enter/exit the beam volume.

For a cylindrical beam

$$A = D_b \pi L \tag{6}$$

In the steady state the left hand sides of Equations (4) and (5) must be equal.

$$\frac{I_e}{e} n_b \sigma L = (n_0 - n_b) A \bar{c} \,/\, 4 \tag{7}$$

from which we can calculate

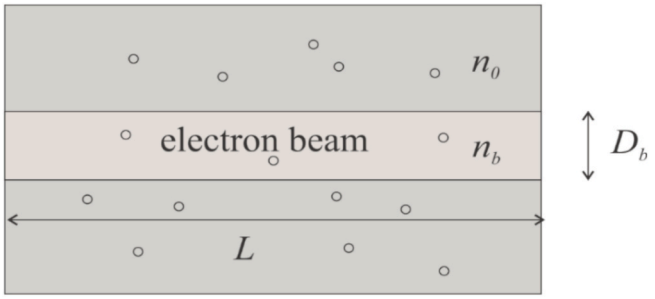

Fig. 2. Side view of a cylindrical electron beam with diameter D_b and length L. The number density of neutral molecules of gas in the beam and outside of it is indicated with n_b and n_0, respectively.

$$n_b = \frac{n_0}{\left(\frac{\frac{I_e}{e}\sigma}{D_b \pi \sqrt{\frac{kT}{2\pi m_p}}} + 1 \right)} \quad (8)$$

with m_p being the particle mass of the neutrals and I_e the electron emission current.

The relative depletion ε is given by:

$$\varepsilon = \frac{n_0 - n_b}{n_0} = 1 - \frac{1}{\left(\frac{\frac{I_e}{e}\sigma}{D_b \pi \sqrt{\frac{kT}{2\pi m_p}}} + 1 \right)} \quad (9)$$

Fig. 4 shows plots of ε as a function of beam diameter for three different gases.

Depending on the electron beam current there is a maximum allowed beam diameter which will keep this systematic error bellow the acceptable limit. For instance, a 1 mA electron beam should have a diameter above 0.1 mm (indicated with the dotted line in Fig. 3) in order to keep this effect below the target of 1%. For a 10 times lower electron current (100 μA) the depletion rate at 0.1 mm diameter reduces roughly by a factor of 10.

2.8. Electron energy distribution

If there is a constant energy of the electrons along their known path of length L through the ionisation volume, the gauge sensitivity for any gas can be predicted using Equation (2) and be compared with experimental results. To achieve this predictability with our design, we aimed at an electron energy with small variations along their path through the ionisation volume.

2.9. Electron stimulated desorption and thermal outgassing around hot filament

The choice of electrode materials and their surface conditions have significant influence on the gauge operation. Electron bombardment onto the Faraday cup surface will produce secondary electrons, ions and photons, but also stimulate desorption of neutrals. An appropriate design must minimize the influence of these effects on the measured ion collector current.

Outgassing of the cathode emitter and heated electrodes near the emitter may affect the lower limit of measurement range of the gauge. Therefore, small and low power cathodes are desirable.

2.10. Ion-induced secondary electron emission from collector

A particularly disturbing effect is the ion induced secondary electron emission from the collector, which has a direct impact on the ion current reading. This effect depends on the actual state of the collector surface and has been investigated in our recent paper [9]. Carbon coating [10] seems to be an efficient way to minimize the instability of secondary electron production by ions. In fact, any surface treatment that roughens the surface such that secondary electrons are trapped by multiple scattering reduces the SEY. Laser ablation [11] is an efficient way to roughen a surface. Another way to reduce the secondary electron emission would be a suppressor grid in front of the ion collector with a potential that pushes the electrons back to the collector [[12,13]]. This, however, complicates the gauge design and we prefer to use a coating for stabilization of the ion-induces secondary electron yield, if deemed necessary.

3. Simulation software used

Four software packages were used to calculate the potentials as well as electron and ion trajectories of potential designs: OPERA, SIMION, COMSOL and WARP. Before using them for design development, all four packages were tested for their suitability to simulate ionisation gauges by comparing the results of their simulations with experimental results of a commercial gauge type, which will not be reported here. It turned out that the WARP software could not be used for simulating an ionisation vacuum gauge [14]. At the beginning, mainly the software programs OPERA and SIMION contributed to the development, while COMSOL was later used to refine the design and investigating its characteristics.

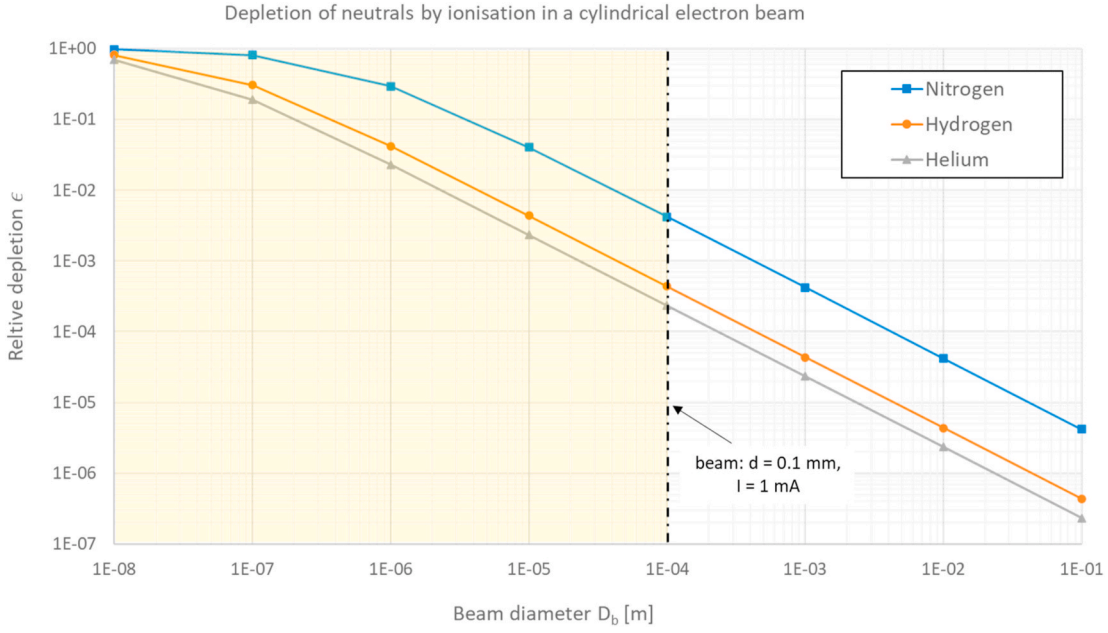

Fig. 3. Relative depletion of neutrals inside a cylindrical electron beam of 1 mA and an energy of 100 eV. The preferred parameter space is outside the yellow area. (For interpretation of the references to colour in this figure legend, the reader is referred to the Web version of this article.)

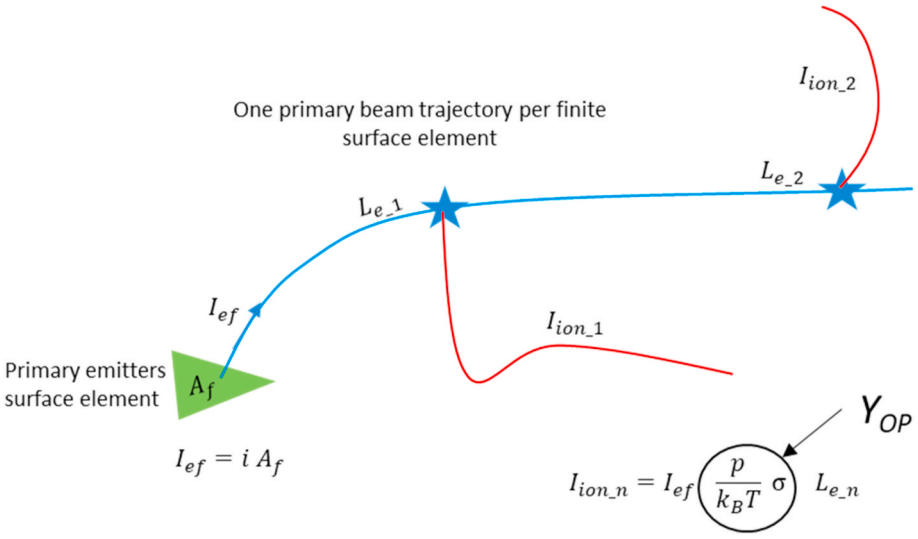

Fig. 4. Charged particle trajectories and trajectory currents used in the simulations in OPERA.

Here, we shortly introduce the basic working principles of these software packages without going into details.

3.1. OPERA

The use of OPERA (www.3ds.com/products-services/simulia/products/opera/) was driven by the fact that it includes space charge effects, which is an important effect to be considered in the simulations. OPERA is a finite element software that calculates charged particle trajectories in electric fields. As illustrated in Fig. 4, one particle trajectory is calculated per finite surface element A_f of the emitting surface. The electron current I_{ef} in each of the trajectories corresponds to the emission current density, an input parameter in the simulations, multiplied by the area of this finite element. Ionisation events, illustrated with a star in Fig. 4, are defined to happen after a trajectory segment length L_{e_n}. The length of the segments varies randomly, but a maximum segment length can be specified in the simulations. The ion trajectories start at the positions of ionisation events. The ion current I_{ion_n} in each of these trajectories correspond to the yield used in OPERA Y_{OP} multiplied by I_{ef} and L_{e_n}:

$$I_{ion\_n} = I_{ef}\, Y_{OP} L_{e\_n} \tag{10}$$

$$Y_{OP} = \frac{p}{kT}\sigma \tag{11}$$

Y_{OP} takes into account the pressure p, temperature T and the impact energy dependent ionisation cross-section σ.

OPERA calculates the modification to the potential field caused by the electrical currents in all the trajectories along the charged particle trajectories by successive iterations. We recently used this software package to characterise the CERN-type modulated Bayard-Alpert gauge. The simulations were in good agreement with the characteristics of that gauge [15].

3.2. SIMION

SIMION ver. 8.1 [16] (https://simion.com/) is a common software for charged particle optics simulations based on solving the Laplace equation by a finite difference method. It is possible to incorporate user codes, written in LUA embeddable scripting language (www.lua.org/) allowing to generate complex initial conditions for electrons and collisions with gas phase neutrals leading to ions whose trajectories can then be followed. The software also allows to introduce a magnetic field and study its effect on the trajectories of charged particles. We wrote a LUA script code to simulate electron-impact ionisation of gas neutrals and electron backscattering from the grid using Monte Carlo approach. This tool was tested to simulate the CERN-type modulated Bayard-Alpert gauge [15], and showed that the results coincide with those obtained by OPERA in the frame of the simulation uncertainty [17].

3.3. COMSOL

COMSOL is a general-purpose finite-element simulation software for modelling designs and processes in various fields of physics and engineering (www.comsol.com). Although a valuable tool to determine potential profiles and charged particle trajectories, COMSOL simulations were only used in the evaluation of the final design. The performed simulations did not include space-charge effects, although COMSOL allows for simulations using them.

3.4. WARP

WARP is an open source Particle-in-Cell (PIC) code written in Python/Fortran. It has been developed for kinetic simulations of particle beams and plasmas. Information about WARP can be found at http://warp.lbl.gov/. It has a wide variety of particle movers and field solvers (electro-static and electro-magnetic). All relevant physics for simulations of ionisation gauges seemed to be implemented. It turned out, however, that the code had inconsistencies, such as target species were not deleted after ionisation [14]. It could therefore not be used for the simulation of the ionisation gauges.

4. Ionisation gauge concepts

In this section we present a selection of four concepts that have been discussed and studied as candidates for a suitable design as an ionisation gauge reference. The initial task for the simulations was to find arrangements that have a chance to meet the requirements. Out of these a final design was chosen, which was further investigated and detailed by simulations. These designs have in common that all the emitted electrons pass the ionisation volume only once in well-defined trajectories and the electrons are intercepted in a Faraday cup at the end of their trajectories. This is the main difference to existing designs as BA-gauge, extractor or triode designs, where the electron path is poorly defined and varying during operation. In addition, in the presented designs, the effect of secondary electrons, ions and photons from the area of electron impingement is largely suppressed. All designs also use electrodes that

guides the emitted electrons into the ionisation chamber. In reference to the design of electron guns and microscopes, we call these electrodes Wehnelt electrodes [18].

4.1. Design with dense and straight focused electron beam ending in faraday cup

The electrons emitted from the filament are directed with a Wehnelt electrode into the ionisation volume (Fig. 5). After passing this volume they enter the Faraday cup on the opposite side. The ions that are generated inside the electron beam are extracted and attracted to the collector, a thin wire on the lower side (Fig. 5). The electric field required to extract the ions also causes a deflection of the electron beam. This design is very similar to the gauge design by Klopfer [19] that we found in our systematic literature review [1].

An arrangement with the associated electrode potential setting of this concept is shown in Fig. 6. The electrons are emitted from a straight filament wire with a limited section (2 mm) coated with low work-function material. This assures that electrons are emitted only from that area if the filament is kept at a relatively low temperature. The electrons are extracted into the ionisation cage due to the potential difference between the filament and the cage. In addition, the coaxial equipotential field around the straight filament also affects the electron trajectories. The latter provides efficient focusing of the electron beam in the direction parallel to the filament axis, as shown in Fig. 6 (right), and guides it through a narrow slot into the Faraday cup. Perpendicular to the filament axis the focusing is much less efficient. The collector in this proposal is a thin ribbon of 20 μm thickness to minimize the view to the Faraday cup opening.

Ion trajectories are short and ions impinge on a rather large surface of the collector. This results in a good stability up to high pressures. Space-charge effects caused by the ion density close to the collector are minimised. Ion losses are in this design caused by the field penetration at the entry and the exit of the ionisation volume (Fig. 7).

At the entrance into the Faraday cup, electrons are deflected such that the electron-impact area is shifted away from the direct line of sight to the collector. This reduces the residual current on the collector caused by photoelectrons, which are generated by X-rays emitted from the electron collisions with the Faraday cup. The deflector also attracts secondary ions generated at the surface by the electron-impact and repels a great part of the low-energy secondary electrons as illustrated in Fig. 8. The trajectories of secondary electrons and ions were simulated with an initial energy perpendicularly emitted from the Faraday cup surface at the area of the impingement of primary electrons. Utilizing such a deflector, the undesired effects caused by the electron impingement on the grid in Bayard-Alpert type gauges are considerably reduced.

Table 1 summarises the performance of this arrangement with respect to mechanical misalignments. As can be seen, in this concept all three performance parameters (electron transmission efficiency, ion collection efficiency and sensitivity) remain stable upon increasing the pressure to 10^{-2} Pa. The requirements with respect to misalignment of the emitter are rather tight.

A drawback of such a geometry with a dense beam is that due to the space-charge within the electron beam, the total emission current is limited to less than 200 μA. However, as can be seen in Table 1, this is sufficient to meet the requirement for minimum collector current as mentioned in section 2.1.

4.2. Design with radial electron emission

Emitting the electrons radially from the centre into a radial-symmetric arrangement reduces the problem of beam defocussing due to space charge and therefore allows higher emission currents. At the same time, such an arrangement can still assure stable and well-defined electron trajectories. This concept is illustrated in Fig. 9. Bills et al. [20] proposed a similar arrangement, in which the emitted electrons pass once radially through a cylindrical ionisation volume. In that geometry, the electrons enter from the outside of the cylinder, but not from the centre as proposed here.

Like in the design described in the previous section, this concept also suggests a partially coated straight filament to assure a well-defined area for the emission of electrons (Fig. 10, right). The current density is rapidly reduced along the beam path, which allows operation with emission currents up to 2 mA without facing space-charge problems. The ion collector has the shape of a ribbon situated at the bottom of the ionisation volume.

The ion trajectories (Fig. 11) are longer than those of the design with straight beam described in the previous section, but are still rather short. Consequently, this concept is also rather insensitive to ion space charge effects at higher pressures. The ion collection efficiency is comparably low with $\varepsilon_{ic} < 0.9$. This is caused by stronger field penetration into the ionisation volume as the electron path length inside that volume is only 19 mm.

This concept makes also use of an electrode (deflector) to attract ions generated inside the Faraday cup and to repel secondary electrons (Fig. 12). Hence, the flux of secondary charged particles into the ionisation volume can be efficiently reduced. It is, however, more difficult to protect the collector against a direct view to the surface where the electrons are hitting the Faraday cup.

Compared to the previous concept, this one is less sensitive to emitter misalignments. Still, alignment tolerances within a few tenths of a millimetre are required (Fig. 13).

This design has a quite low sensitivity ($S = 0.097$ Pa^{-1}) with respect to the device dimensions. In this layout the ionisation cylinder has an

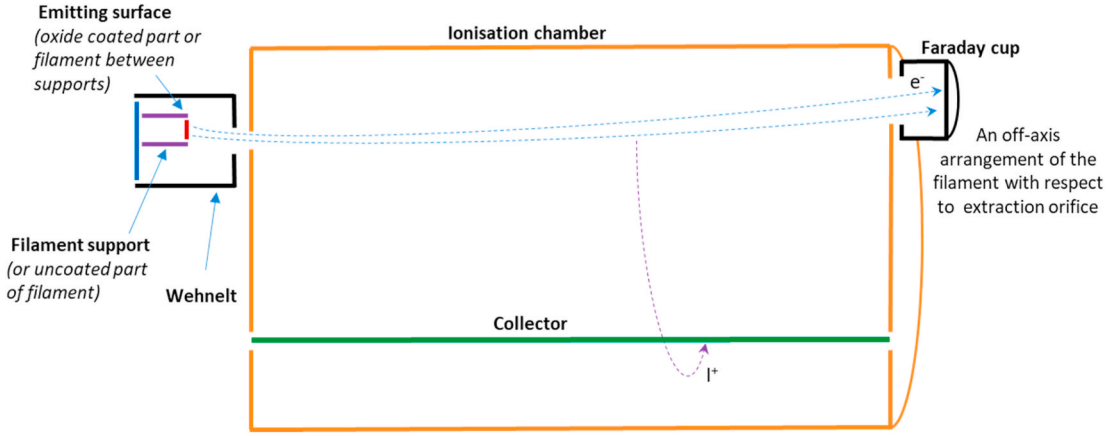

Fig. 5. Basic concept of an ionisation gauge with a single beam.

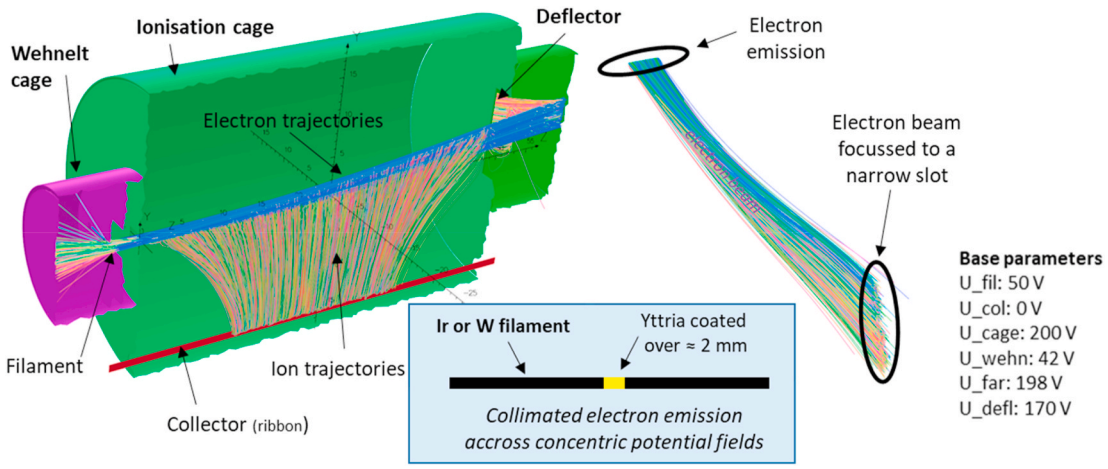

Fig. 6. Design following the concept shown in Fig. 5, with details of the emitter and the change of the beam cross-section along the electron trajectories.

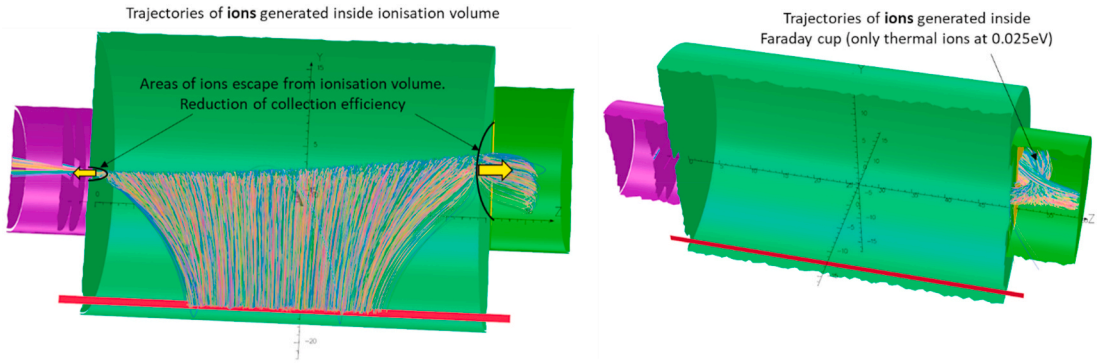

Fig. 7. Field penetration into ionisation volume (left) and ion trajectories in the Faraday cup.

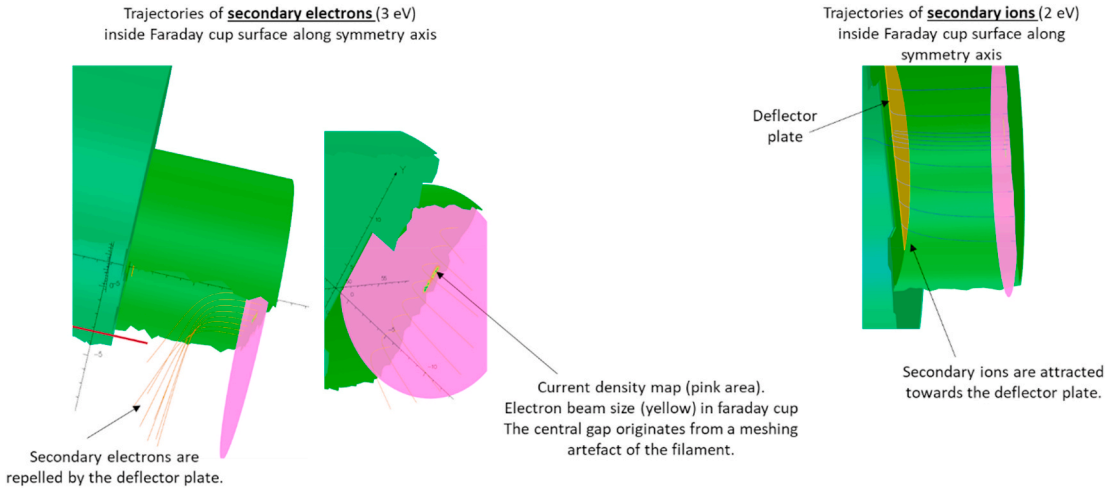

Fig. 8. Trajectories of secondary particles originating from the surface where the primary electrons are impinging.

external diameter of 50 mm. Increasing the sensitivity by increasing the electron path length to have a comparable sensitivity as in the previous concept, would result in a quite space consuming device.

Table 2 summarises the performance of the arrangement shown in Fig. 10. As can be seen, the performance parameters are also stable within a reasonable range of emitter misalignments.

4.3. Design with larger straight electron beam ending on a target plate

The two previous layouts required rather precise alignments of the electrodes, comparable to the demands in electron guns and residual gas analysers. The layout presented in this section has the advantage to allow much higher mechanical misalignments. The electrons are emitted from a rather long section of the filament, pass the ionisation volume once, and hit a target plate.

Partial coating of the filament would not be necessary and the

Table 1
Performance of the single beam arrangement with Faraday cup shown in Fig. 6. If not otherwise mentioned values are simulated at 10-6 Pa.

	Electron current at Faraday cup [A]	Electron transmission efficiency	Ion current at collector [A]	Ion collection efficiency	Sensitivity [Pa^{-1}]
Base parameters	4.40E-05	0.998	1.26E-11	0.930	0.2854
Increase el. emission at source: +100%	8.46E-05	1.000	2.43E-11	0.934	0.2867
dV_filament: +1 V (filament potential)	3.91E-05	0.998	1.12E-11	0.933	0.2857
dZ_filament = +0.2 mm (long.)	5.46E-05	0.886	1.78E-11	0.938	0.2882
dZ_filament = +0.1 mm (long.)	5.18E-05	0.998	1.48E-11	0.930	0.2855
dZ_filament = −0.1 mm (long.)	3.39E-05	1.000	9.60E-12	0.920	0.2833
dY_filament = −0.1 mm (vert.)	4.45E-05	0.999	1.27E-11	0.933	0.2854
dX_filament = +0.1 mm (lat.)	4.25E-05	1.000	1.21E-11	0.926	0.2852
Pressure: 10^{-2} Pa	4.56E-05	0.998	1.29E-07	0.924	0.2821
V_defl: 0 V	4.46E-05	0.995	1.19E-11	0.867	0.2658

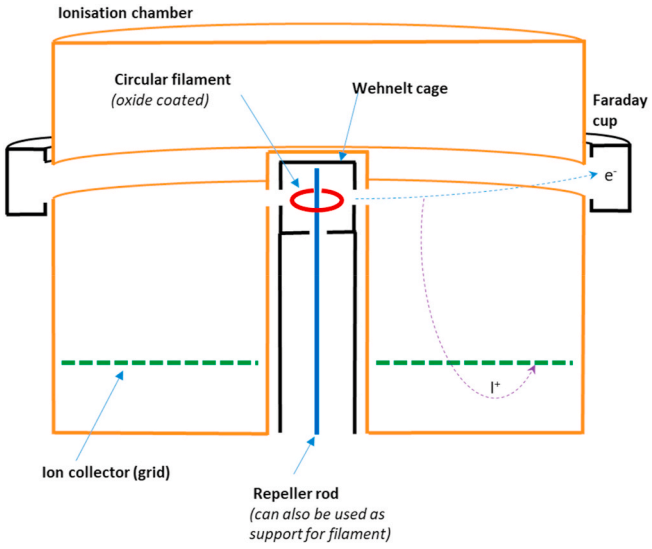

Fig. 9. Concept with radial-symmetric electron emission.

Wehnelt electrode is fixed to ground potential. It shields the two collectors from ions generated outside the ionisation volume. The two collector rods are installed close to the grid and serve as a guide for the electrons. A second grid around the grid of the ionisation volume, at the same potential, minimises field penetration from the surrounding vacuum chamber and acts as a barrier for ions, which would be otherwise lost once they pass the first grid (Fig. 14). This allows to mount the collectors very close to the grid, whilst keeping the ion collection efficiency high. Most of the lost ions are leaving through the entry and the exit grid. The transmission for electrons is reduced since they must cross the two grids (having 95% transparency each). This means that still around 10% of the electrons hit the grid at maximum energy. The instability problems of traditional Bayard-Alpert type gauge caused by the electron impingement onto the grid are in this configuration reduced but cannot be suppressed.

The electrons hit the target at low energy of a few electron-volts only. Below an impingement energy of 10 eV, the energy of most of the photons generated on the target is too low to generate photoelectrons at the collector [21]. The secondary electron yield is also considerably reduced. However, at low incident energies the portion of reflected electrons increases [22]. Therefore, the target should not be simply a plate as shown here but structured in a way to secure multiple reflections of impinging electrons and ultimately getting them absorbed. An additional suppressor electrode may be required. Table 3 summarises the performance of the arrangement shown in Fig. 14. The length of the ionisation volume and its potential are the same as for the one described in section 4.1.

4.4. Design with cylindrical belt-like beam

Following the concept shown in Fig. 15, inspired by cylindrical energy analysers, electrons are emitted from a linear filament oriented along the axis of the two concentric cylindrical electrodes that are used to accelerate and deflect the electron beam. The field distribution provides focusing of electrons in the deflection plane. Normal to this plane there is no potential gradient, such that the electron beam has a shape of a belt. In a modification of this design, a deflection electrode bends the belt-shaped beam through a slit into the cylindrically shaped Faraday cup situated inside the inner electrode (Fig. 16). In front of the ion

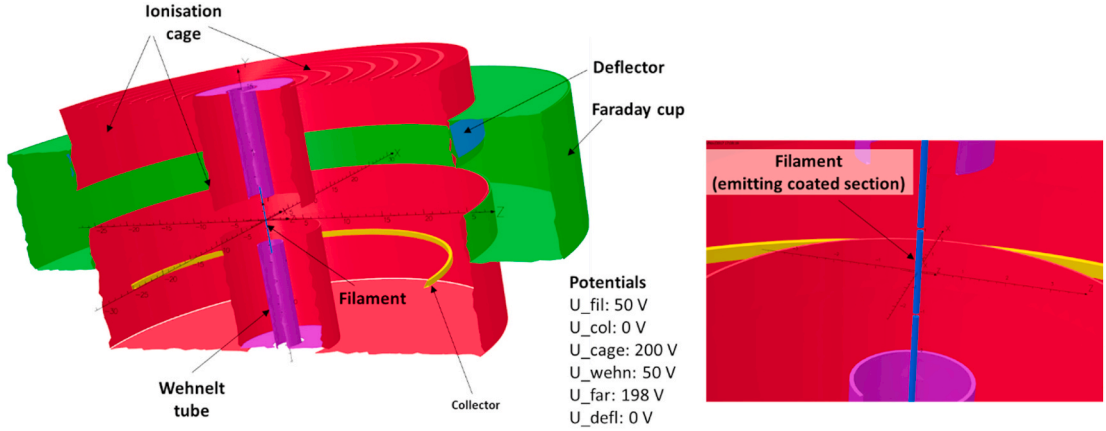

Fig. 10. Design of an ionisation gauge with radial-symmetric electron emission.

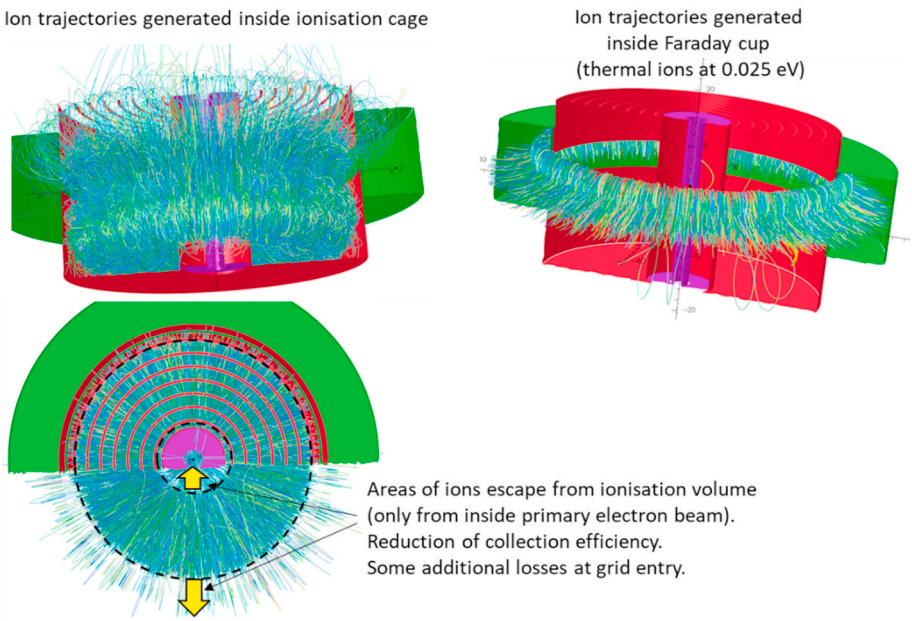

Fig. 11. Ion paths. The dotted lines indicate the separation of collected and repelled ions.

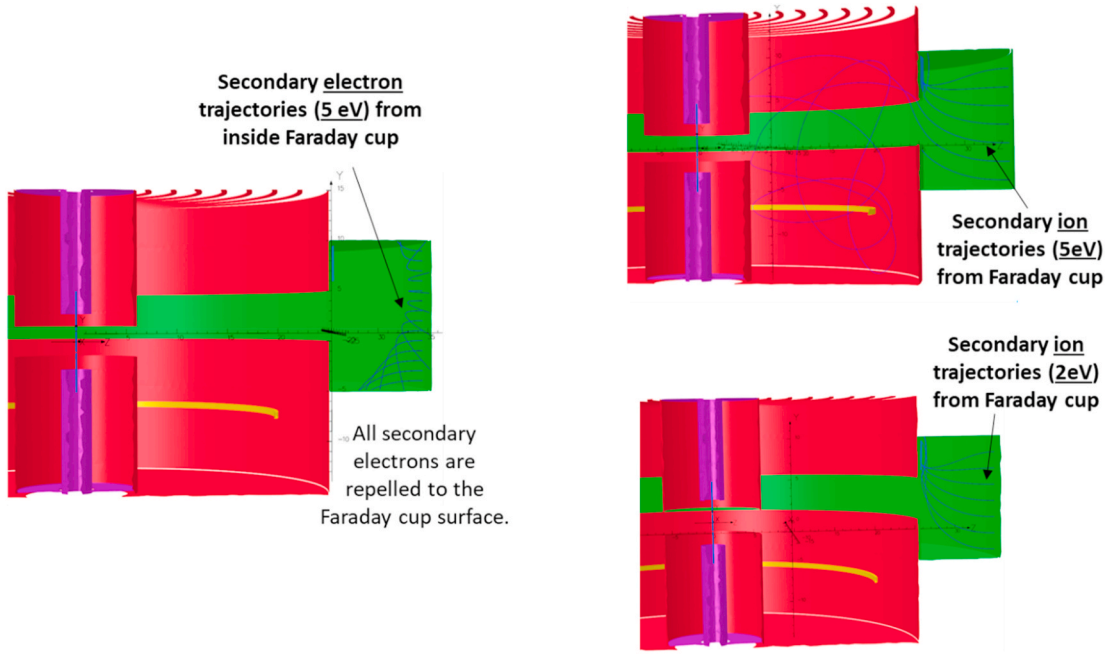

Fig. 12. Trajectories of secondary charged particles.

collector, which represents a central section of the outer electrode, there is a grid which suppresses ion induced secondary electron emission. The main advantages of this concept are the absence of ion-induced secondary electron yield, highly reliable collection of the primary electrons and no direct sight of electron impinging sites to the collector. At the same time, the sensitivity of the gauge is rather low (around 0.09 Pa^{-1} for N_2) caused by an ion collection efficiency ε_{ic} of only 17%. Similar as the radial-symmetric concept presented in section 4.2, this device will require rather large radial dimensions.

5. Chosen design

5.1. Description of the design

Our choice of the ionisation gauge reference standard corresponds to the design with the dense and straight focused electron beam as described in section 4.1, but with further improvements and optimisation. The reason for this choice is that we can apply rather conventional electron beam optics, similar to those of electron guns, and that the electrons adopt parallel trajectories entering the Faraday cup through a small opening. This makes it easier to suppress secondary electrons, ions and photons than with the designs described in section 4.2 and 4.3. The chosen design has also a higher sensitivity compared to the designs described in sections 4.2 and 4.4 while keeping the lateral dimensions

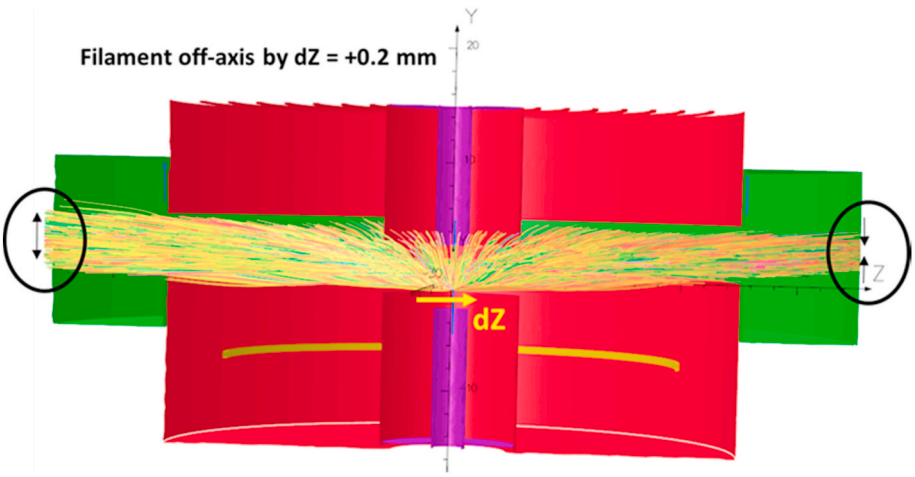

Fig. 13. Influence of an off-axis positioning of the emitter.

Table 2
Performance parameters of a design following the radial-symmetric concept.

	Electron current at Faraday cup [A]	Electron transmission efficiency	Ion current at collector [A]	Ion collection efficiency	Sensitivity [Pa^{-1}]
Base parameters	9.36E-04	0.995	9.14E-11	0.883	0.0972
dV_filament: +1 V (filament potential)	9.36E-04	0.994	9.10E-11	0.879	0.0967
Increase el. emission at source: +100%	1.88E-03	0.998	1.83E-10	0.882	0.0970
Pressure: 10^{-2} Pa	9.36E-04	0.994	9.20E-07	0.889	0.0978
dZ_filament = +0.2 mm (off axis)	9.35E-04	0.993	9.11E-11	0.873	0.0968
dY_filament = +0.3 mm (axial)	9.04E-04	0.960	9.29E-11	0.895	0.0987
dY_filament = −0.3 mm (axial)	9.41E-04	1.000	9.04E-11	0.869	0.0961

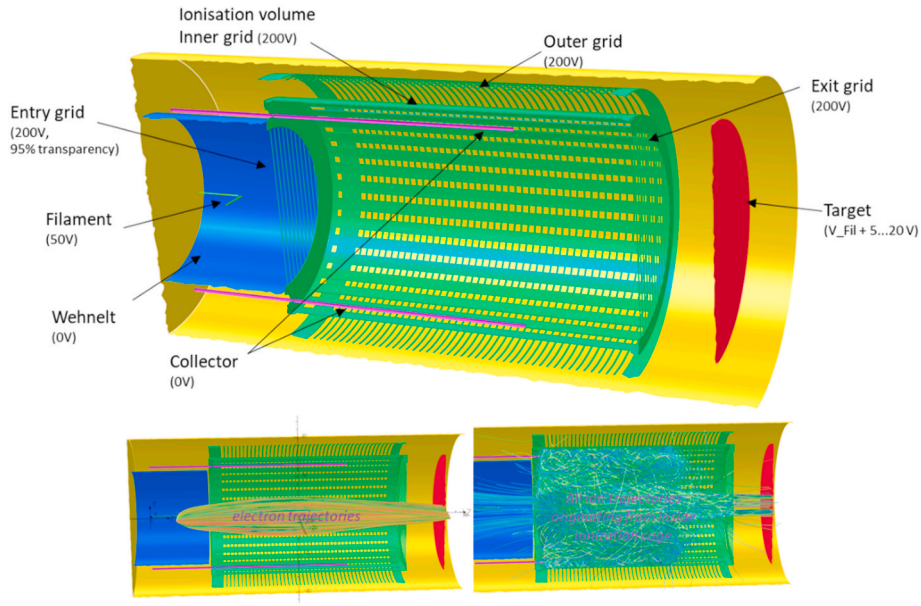

Fig. 14. Design following a single beam concept, allowing larger alignment tolerances (cut through symmetry axis).

reasonably small.

Fig. 17 shows the design of the gauge with its nominal potentials and Fig. 18 gives the most relevant dimensions. Instead of using a partially coated filament as an emitter, we chose to use commercially available, directly heated emitters. The emitting element is a small disk with a diameter of 0.84 mm. The energy spread of the electrons leaving the emitter is less than one eV [23]. The arrangement of the emitter, Wehnelt and ionisation cage entry provides efficient extraction of all emitted electrons in the form of a parallel beam. The electron beam passes through the ionisation volume and enters the Faraday cup assembly where it is deflected by about 150°. Therefore, no X-ray photons enter the ionisation volume directly from the electron impingement area providing flexibility for the collector design and position. The collector in this design has two functions. One is its usual function of ion

Table 3
Performance of a single beam arrangement with larger alignment tolerances.

	Electrons emitted [A]	Electron transmission efficiency	Ion current at collector [A]	Ion collection efficiency	Sensitivity [Pa^{-1}]
With base parameters at p = 10^{-6} Pa	5.00E-04	0.888	1.43E-10	0.979	0.2864
Pressure p = 10^{-2} Pa	5.00E-04	0.887	1.44E-06	0.981	0.2877
dZ_filament = - 1 mm (increase distance to grid)	2.64E-04	0.885	7.56E-11	0.974	0.2859
dZ_filament = + 1 mm (increase distance to grid)	5.00E-04	0.892	1.42E-10	0.976	0.2847
dX_filament = +1 mm (lateral)	4.72E-04	0.896	1.36E-10	0.980	0.2890
dY_filament = +1 mm (vertical)	4.93E-04	0.891	1.41E-10	0.981	0.2858
dV_filamen t = −5 V, (p = 10^{-2} Pa)	5.00E-04	0.872	1.41E-06	0.980	0.2815
Increase el. emission (p = 10^{-2} Pa)	1.57E-03	0.897	4.49E-06	0.882	0.2871

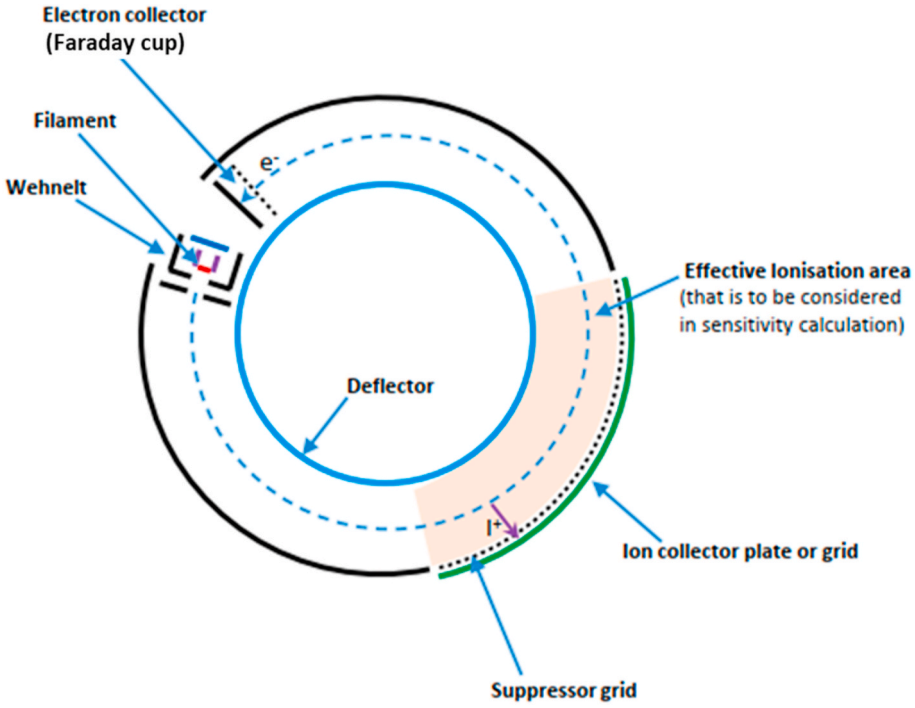

Fig. 15. Concept with of a bent-belt electron beam.

extraction and collection. The other function is the focusing of the electron beam into the Faraday cup entry. This feature confines the beam at the exit and hence increases the tolerance for emitter misalignments. However, it has the inconvenience that it introduces a potential dip along the electron path inside the ionisation volume, resulting in a variation of the ionisation cross-section.

While the escape of low energy electrons from the Faraday cup is efficiently suppressed by the deflecting electrode, some of the more energetic electrons can still leave the Faraday cup (Fig. 17, bottom right).

The length of the tubular extension at the ionisation cage exit, as well as the shape and thickness at the ionisation cage entry are chosen such that, with nominal settings, the maximum field penetration from the extremities coincide with the entry and the exit plane. These planes then also define the ionisation region (Fig. 17, bottom left). The ion collection efficiency is defined as the number of ions collected divided by the number of ions generated between these planes. $\varepsilon_{ic} = 1$ means that all of the ions between these planes, and only those, are reaching the collector. With this definition, ε_{ic} can be greater than 100% in the case that ions from outside this region reach the collector.

The simulations of this design performed by OPERA, SIMION and COMSOL agree very well. For instance, at a gas temperature of 300 K, the calculated sensitivities for N_2 are 0.288 Pa^{-1} (OPERA, Fig. 17), 0.297 Pa^{-1} (SIMION, Fig. 19) and 0.281 Pa^{-1} (COMSOL, Fig. 20). Interestingly, by applying Equation (2) and knowing that the electron energy in the 50 mm long ionisation volume is approximately constant (200 eV), the calculated sensitivity is 0.281 Pa^{-1}. The small discrepancy can be explained by the non-constant electron energy inside the ionisation volume. Hence, Equation (2) is a very good estimation of the gauge sensitivity just from the gauge geometry and the applied voltages.

More important for the final goal of this work is that, according to the simulations, the whole assembly is rather robust. The ranges of different parameters, including mechanical misalignments, in which the simulations predict stable performance within the target precision of 1%, are summarized in Table 4. These results encouraged us to proceed with the realisation of the ionisation gauge based on this design.

5.2. Discussion on variations of parameters

In the following we discuss in more details variations of different gauge parameters, such as sensitivity, ion collection efficiency and electron transmission efficiency, with gas pressure, electrode voltages, mechanical misalignments, and stray magnetic fields. In addition, the influence of the shape of the electron emitter and its bombardment by energetic ions will be discussed. The simulations were performed by means of both OPERA and SIMION providing very similar results. The

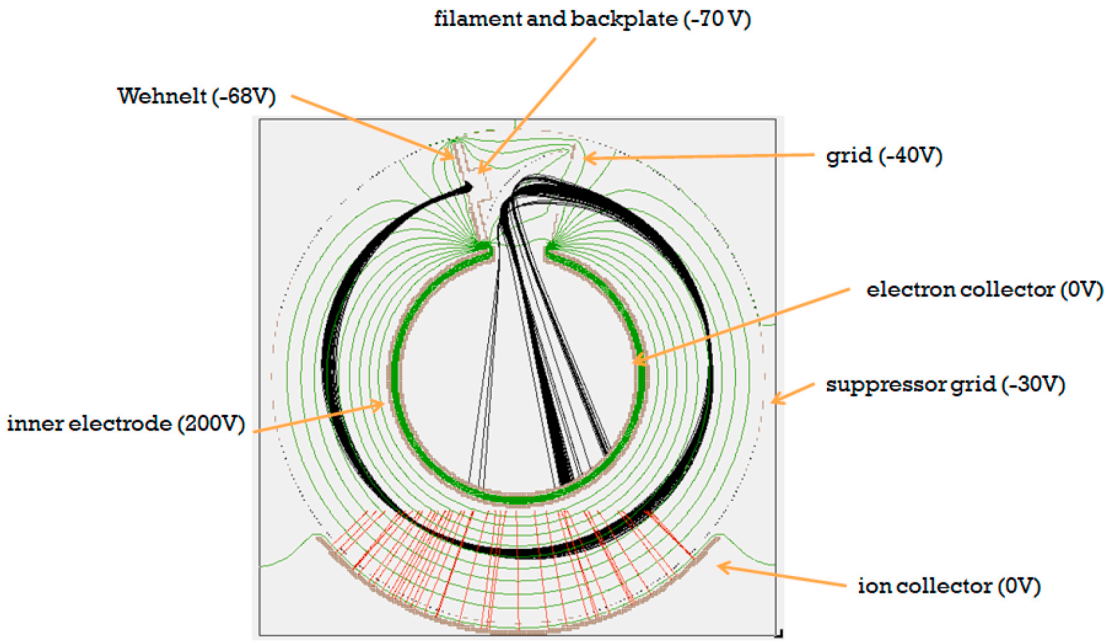

Fig. 16. Design with a bent-belt beam, with calculated electron (black) and ion (red) trajectories. (For interpretation of the references to colour in this figure legend, the reader is referred to the Web version of this article.)

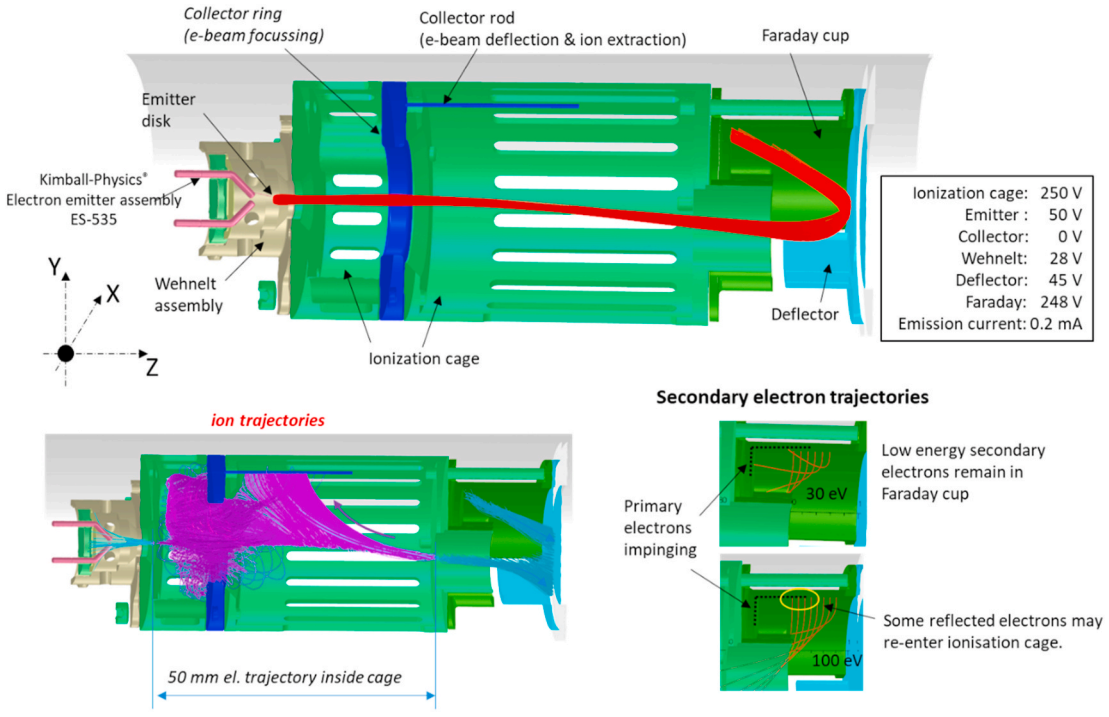

Fig. 17. Design and charged particle trajectories of the gauge following the design described in section 4.1, after further improvements and optimisation.

presented results are obtained by OPERA, unless otherwise stated.

5.2.1. *Variation of pressure*

Fig. 21 shows that the gauge sensitivity remains stable up to the maximum design pressure of 10^{-2} Pa. The simulation in OPERA does not take into account the mean free path of neutrals and collisions of ions with neutrals. The early decrease in sensitivity for pressures higher than 10^{-2} Pa in the simulation shown here is caused by ion space-charge. Whilst the electron transmission is still at 100% at higher pressures, the collection efficiency and sensitivity decrease. The number of positively charged ions inside the electron beam close to the entry and exit causes a shift of the penetration field further into the ionisation volume. The boundary at which ions are collected or repelled moves with this shift. By reducing the emission current at higher pressures, this effect can be reduced, and the pressure range is a bit extended. However, at 10^{-1} Pa the ionisation yield per electron (see Equation (4)), which can also be interpreted as the ratio of the sum of ionisation cross-sections occupied by all neutrals inside the beam and the beam area, is of the order of 3%. This means that the probability of overlapping cross-sections of molecules becomes non-negligible. Therefore, extending

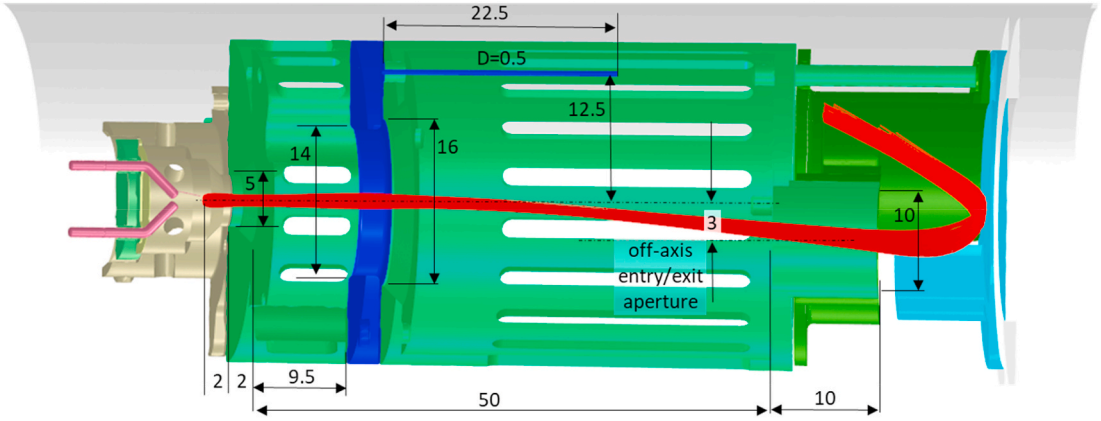

Fig. 18. Essential dimensions of the gauge in mm.

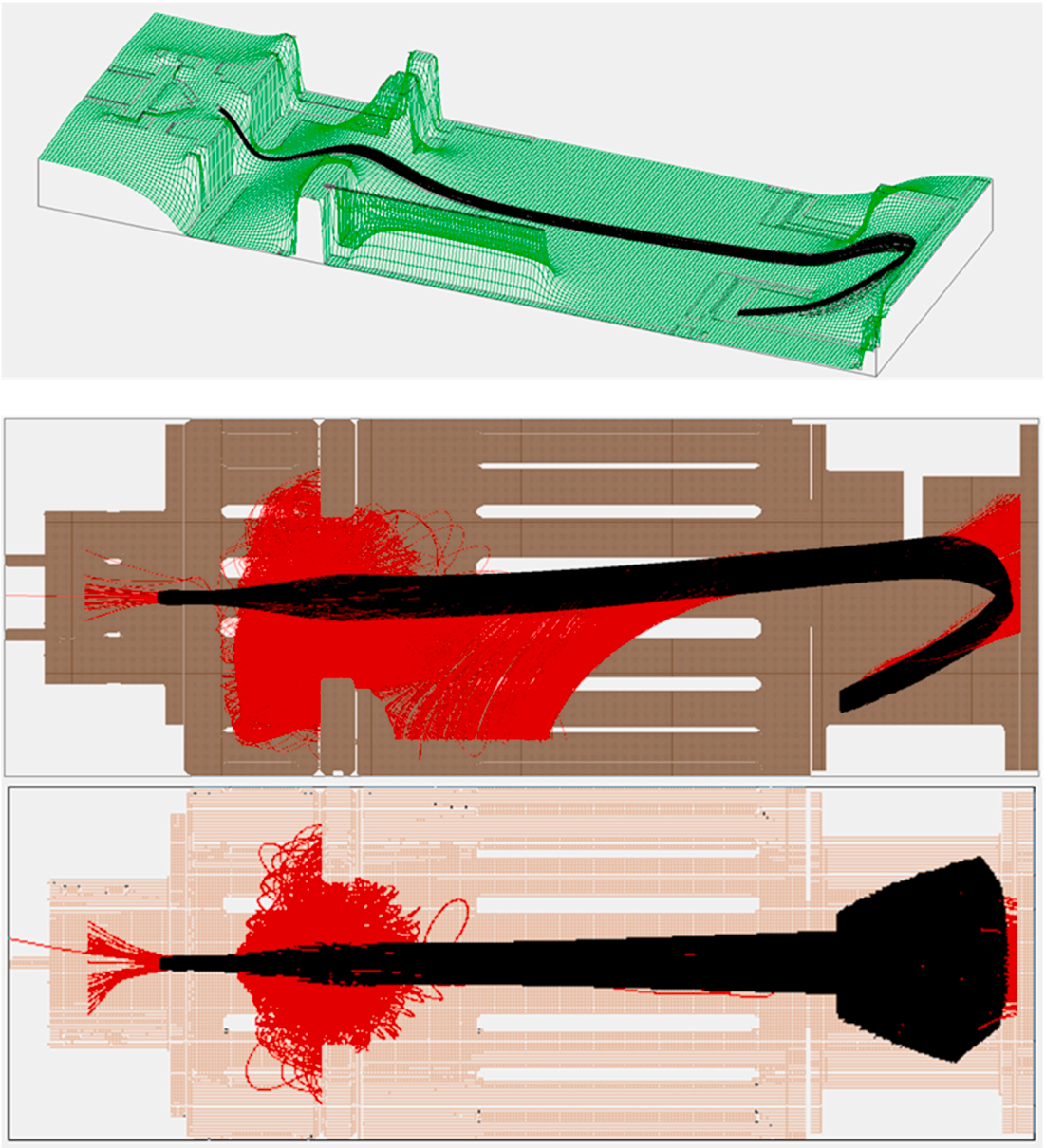

Fig. 19. Simulation of the gauge with SIMION. Electric potential surface for electrons (top) and electron trajectories (black) and ion trajectories (red) from two different views (X and Y as defined in Fig. 17) under nominal potentials. (For interpretation of the references to colour in this figure legend, the reader is referred to the Web version of this article.)

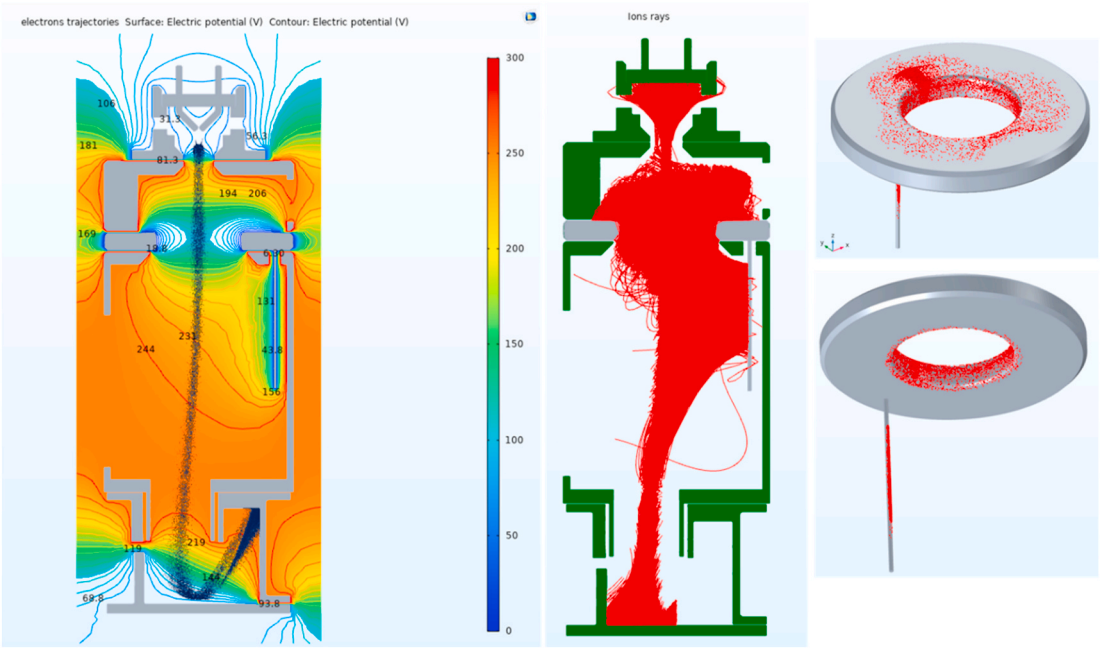

Fig. 20. Simulation of the gauge with COMSOL. Electron trajectories and potential lines (left), ion trajectories (centre) and ion impingement on collector (right).

Table 4
Ranges with performance parameter changes within less than 1%.

Parameter	Range
Pressure	10^{-6} … 10^{-2} Pa
Emitter potential	49 … 51 V
Emission current [mA]	0 … 0.5 mA
Emitter misalignment dZ (long.)	−0.5 … +0.5 mm
Emitter misalignment dY (vertical)	−0.4 … +0.4 mm
Emitter misalignment dX (lateral)	−0.3 … +0.3 mm
Emitter plane angular misalignment	−20° … +20° (X and Y rotation)
Wehnelt misalignment dZ (long.)	−0.1 … +0.1 mm
Wehnelt misalignment dY (vertical)	−0.1 … +0.1 mm
Wehnelt misalignment dX (lateral)	−0.1 … +0.1 mm
Collector ring misalignment dY (vertical)	−0.25 … +0.45 mm
Collector ring misalignment dX (lateral)	−0.2 … +0.2 mm
Collector rod bent	−4° … +4° (X and Y plane)

the operation range with the given dimensions will have limitations if linearity below 1% is required.

5.2.2. *Variation of the emitter potential*

In most of the simulations in OPERA the initial energy of the electrons at the start of their trajectories was taken as 0.1 eV. Varying the emitter potential (Fig. 22), we test whether all electrons within the energy spread of the emitter follow the same trajectories.

In addition, control of the emission current is done by adjusting the heating current through a heating wire. A change of heating current causes also a change of the filament (and consequently emitter) potential.

5.2.3. *Variation of emission current*

The control parameter for the emission current is the emission current density across the whole specified emitter surface. However, due to the potential distribution, not the entire emitter may effectively emit electrons. Due to the potential configuration of the electrodes and space-charge caused by the electron beam close to the emitter, electrons may

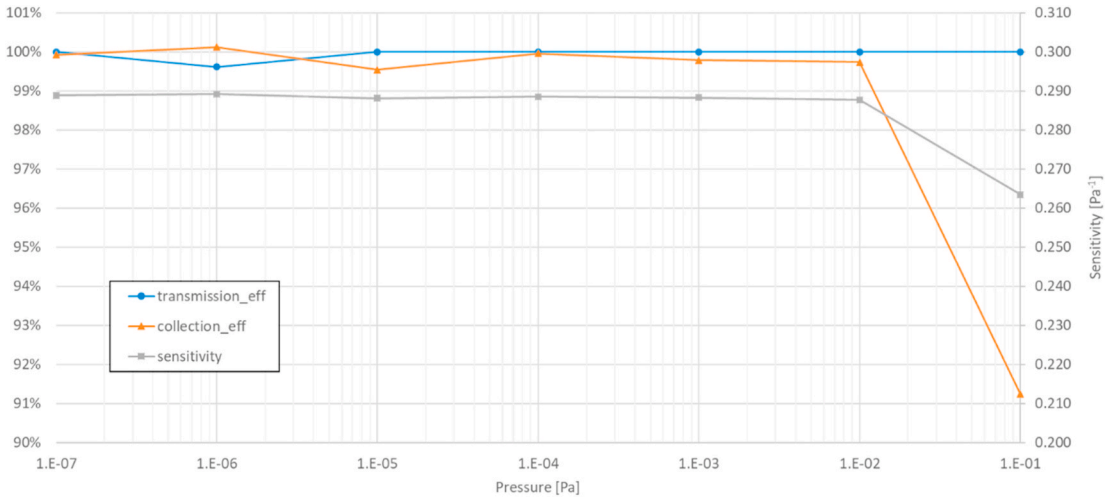

Fig. 21. Variation of pressure.

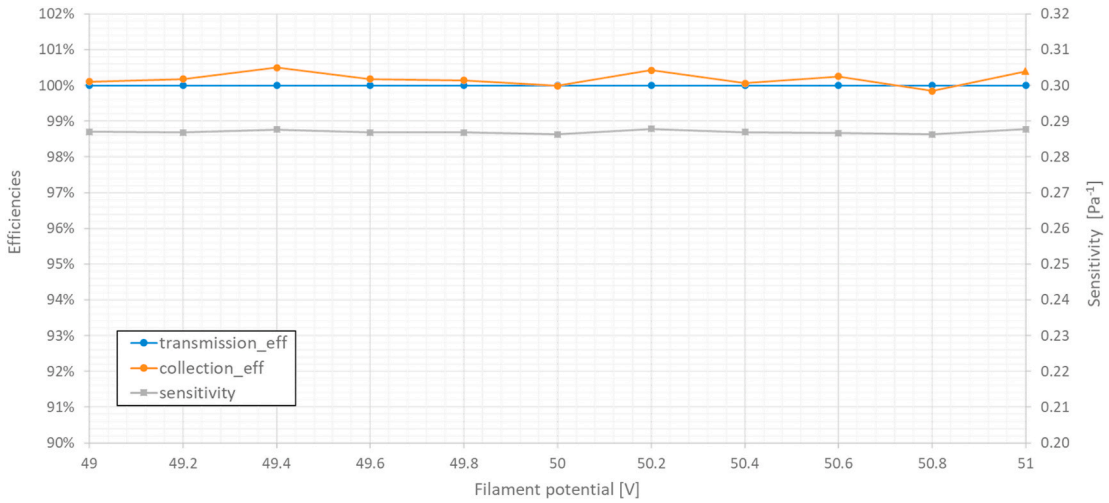

Fig. 22. Variation of the emitter potential.

not be able to leave and are immediately pushed back into the emitter. The effective emission current is therefore not necessarily proportional to the specified emission current density. In Fig. 23 we varied the emission current density by OPERA. The left graphs show the evolution of the performance parameters and on the right the corresponding emission current. The deviation from the direct proportionality in the right graph is due to space-charge. The fact that only the transmission is affected means that most of the effectively emitted electrons pass the ionisation volume within the trajectory envelope, but do not reach the Faraday cup. In the simulation, some electrons hit the tubular extension at the entry into the Faraday cup.

5.2.4. *Faraday cup potential*

The Faraday cup potential has only little effect on the gauge performance parameters (Fig. 24). Depending on the secondary electron yield and energy distribution the Faraday potential can therefore be adjusted to reduce the number of secondary electrons (mainly those at higher energies) entering the ionisation cage. The increase of the ion collection efficiency to greater than one is caused by a small shift of the penetration field towards the exterior of the ionisation volume boundaries described in section 5.1.

5.2.5. *Emitter positioning*

In this design the emitter is a disk spot-welded on a thin heating wire, both reaching temperatures above 1500 K. Because of thermal movements and the fragile structure, assuring precise position of the emitter disk inside the Wehnelt assembly in all directions within 0.1 mm is difficult, even though the emitter manufacturer (Kimball Physics) states rather precise manufacturing tolerances. Fig. 25 shows the acceptable alignment tolerances for displacements along the X-axis (lateral). At a displacement higher than 0.3 mm the transmission decreases, but the sensitivity and collection efficiency remain stable. The electrons still pass through the ionisation volume in stable trajectories, but not all electrons reach the Faraday cup. Even though the sensitivity is not affected in the simulations, the decrease of electron transmission can provoke significant detrimental effects on the collector current reading due to X-rays, secondary electrons and ions. We therefore consider for the allowed misalignment range only that range in which the electron transmission is still stable.

The acceptable misalignments in the Y and Z direction are ±0.4 mm and ±0.5 mm, respectively, and the overall trend is similar.

5.2.6. *Angular alignment of emitter disk*

With the simulations shown here, we check the performance against a misorientation of the emitter plane. Fig. 26 demonstrates that the gauge performance parameters are not affected within at least ±20° when the disk is rotated along an axis parallel to the X-axis. Due to the near cylindrical symmetry, the behaviour is similar for rotations along an axis parallel to the Y-axis.

5.2.7. *Wehnelt – cage relative alignment*

At the entry into the ionisation volume, the electrons pass two cone-

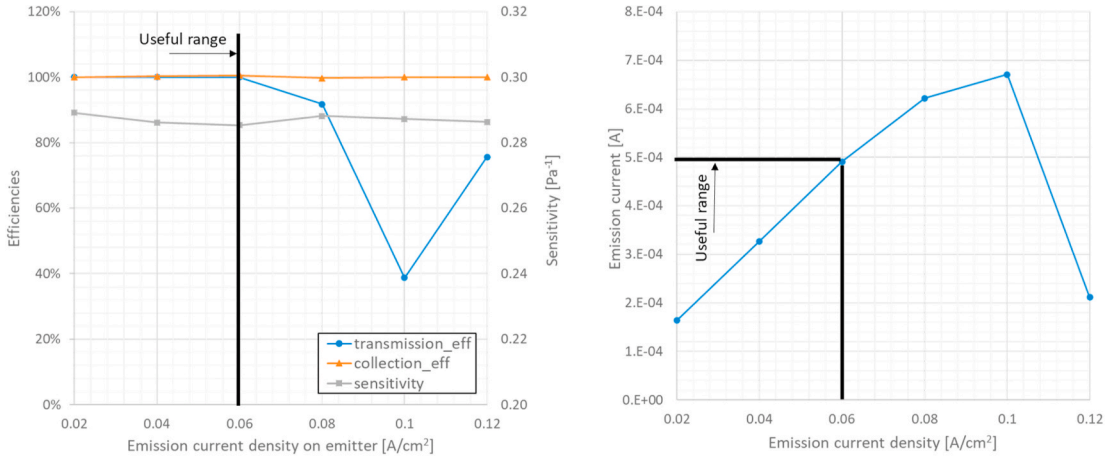

Fig. 23. Variation of emission current density.

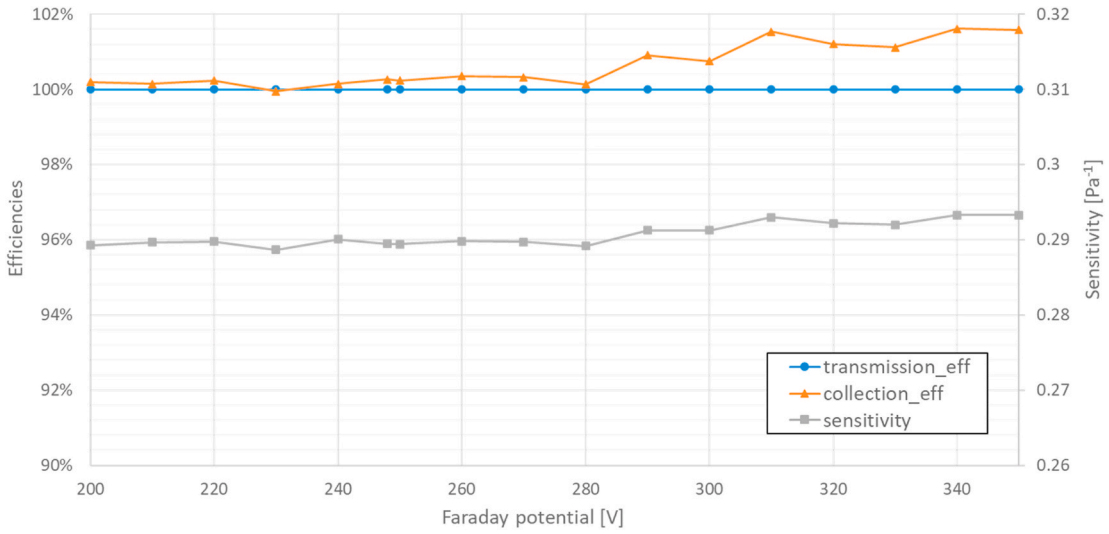

Fig. 24. Efficiencies and sensitivity with Faraday potential.

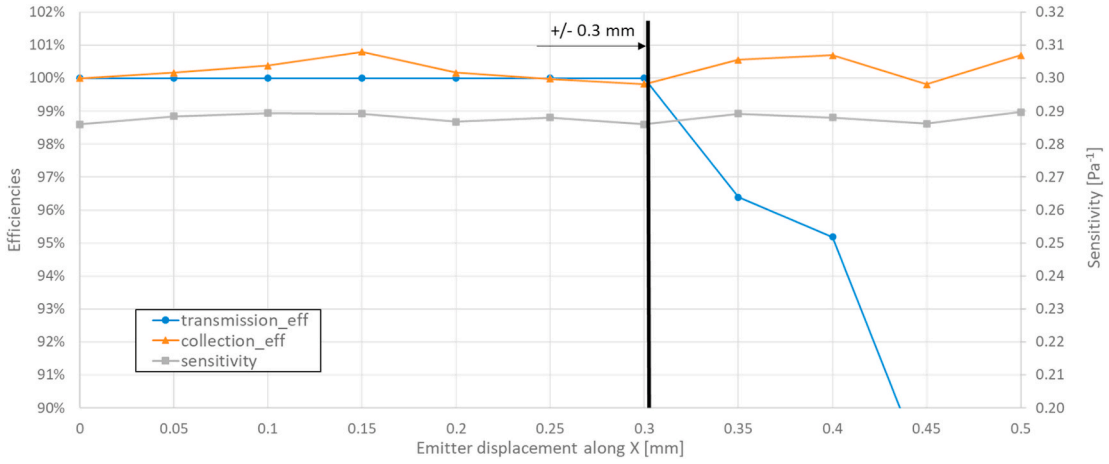

Fig. 25. Emitter misalignment along X-axis (lateral). Because of symmetry, only positive misalignments have been simulated.

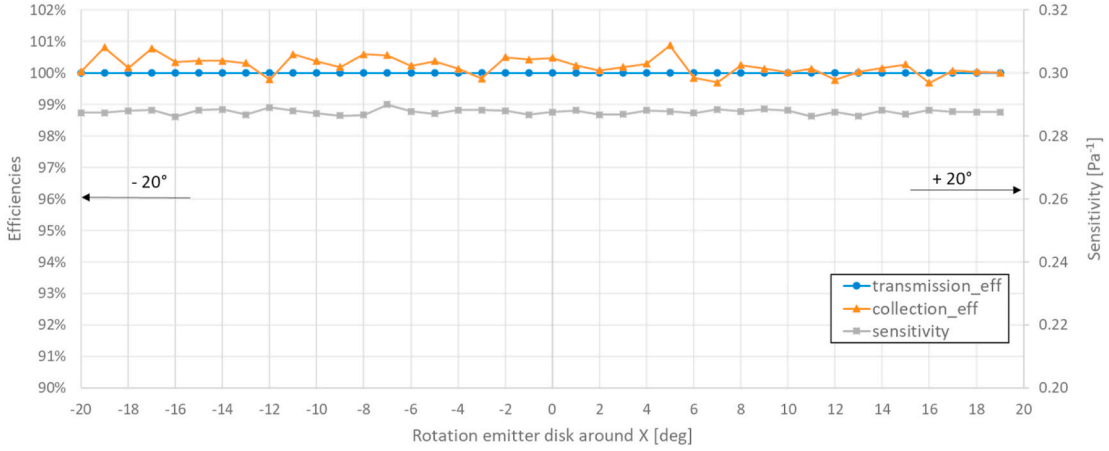

Fig. 26. Emitter disk angular misalignment (rotation of the disk along an axis parallel to the X-axis).

shaped apertures of the same inner diameters. The alignment of these lenses with respect to each other must be within ±0.1 mm in all directions (Fig. 27). This is achievable for such dimensions and alignment configuration with standard machining and alignment technologies.

5.2.8. Collector ring – cage relative alignment

A misalignment of the collector ring causes a displacement of the electron beam at the exit. The collector ring must be aligned within ±0.2 mm (Fig. 28). Exceeding this value, the transmission of electrons is

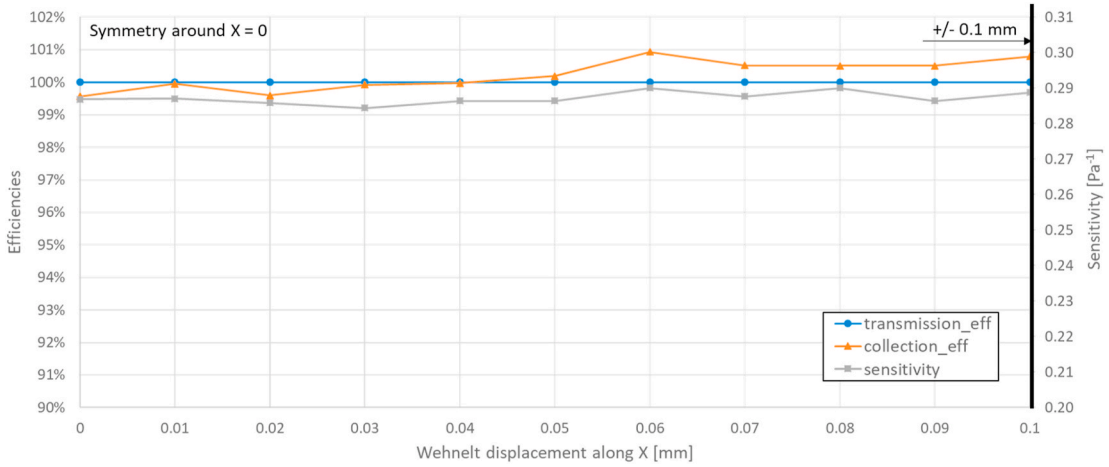

Fig. 27. Wehnelt-cage relative alignment. Because of symmetry, only positive misalignments have been simulated.

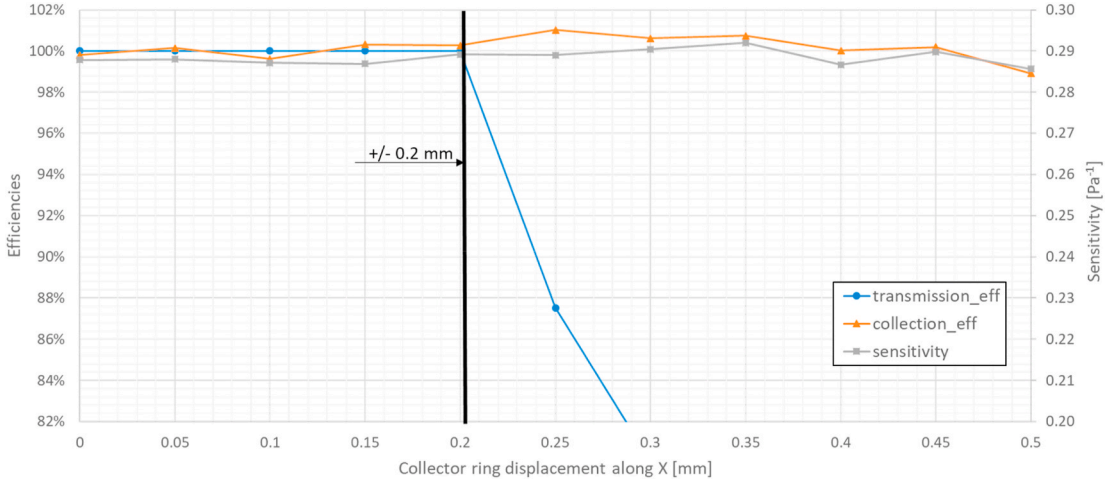

Fig. 28. Collector ring – Cage relative alignment along the X-direction. The position of collector ring is changed in the simulations. Because of symmetry in this direction, only positive values are shown.

greatly reduced. The behaviour in X-direction differs from the one in Y-direction. The sensitivity, however, appears not be affected by such a misalignment. In the negative Y-direction at around −0.4 mm the sensitivity even increases up to 0.34 Pa^{-1} within a small range of Y-displacements (Fig. 29). This is caused by the reflection of electrons back into the ionisation volume (detail A in Fig. 29).

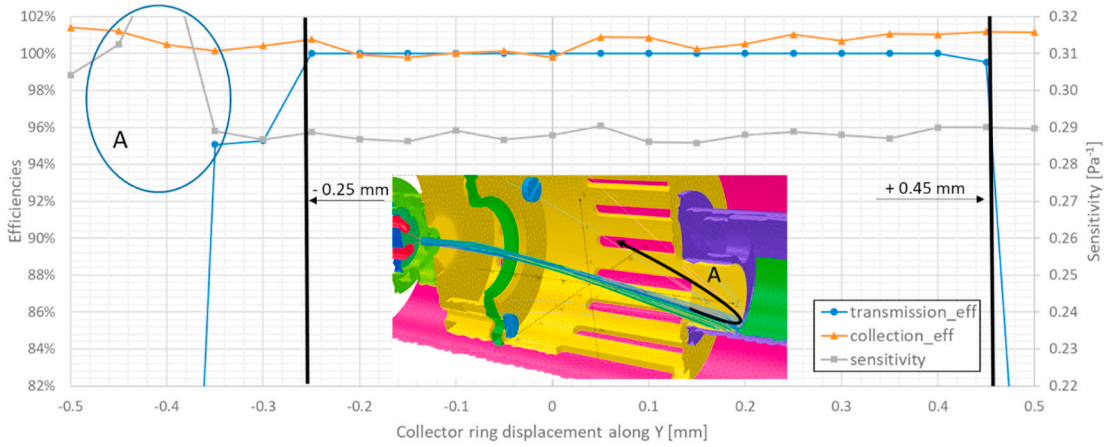

Fig. 29. Collector ring - Cage relative alignment along the Y-direction. The picture in the graph shows the position of the electron beam at which electrons are reflected back into the ionisation volume (indicated with the letter A). Around this position, the sensitivity increases above the nominal value (highlighted with the oval in the graph). The thick vertical lines indicate the range within which the sensitivity and electron transmission remain stable within ±1%.

5.2.9. Collector rod angular alignment

The collector rod can be quite precisely positioned on the collector ring. The tolerance of this position was therefore not investigated. The perpendicular orientation of this rod with respect to the collector ring, however, is more difficult to control. Fig. 30 shows that within an angle of 4° a bent rod along the Y-direction has no considerable impact on the performance. This is also true along the X direction. 4° correspond to a displacement of the extremity of more than 1 mm.

5.2.10. Multi-parameter evaluation of gauge sensitivity

The effect of the simultaneous variation of multiple parameters (e.g. position of collector ring, emitter, Wehnelt) on the sensitivity was investigated by means simulations. A factorial design (FD) of 61 extra simulations was set-up to investigate the significance of variations in input data and to evaluate if there are correlated effects in the corresponding sensitivity of the ionisation gauge. In the multi-parameter study the variations are taken from initial simulations where collector efficiency is close to 100%, thus if the variation in misalignments are larger these effects may significantly increase. It is indicated that the y-position of the collector ring may have a significant influence, whereas all the other parameters seem to have small effects on the sensitivity. No significant correlations between the parameters were observed. We need to point out here that only physical misalignments of certain components were investigated, not variations of potential. The results indicate that in production the components must be fitted rather carefully to give the expected sensitivity of the IG instrument.

5.2.11. Ion impingement on the emitter

Before entering the ionisation volume, the electrons have already enough energy to ionise residual gas. Most of the ions created in this zone are accelerated onto the emitter. Fig. 31 shows the position of the impacts on the emitter disk. At the maximum operation pressure of 10^{-2} Pa and an emission current of 0.2 mA, the ion impingement current corresponds to $1.2 \cdot 10^{-8}$ A. The ion current generated inside the ionisation volume and collected on the collector under the same conditions is of $5.6 \cdot 10^{-7}$ A. The great majority of the impinging ions has energies between 100 eV and 150 eV, which is sufficient to sputter material from the disk except in the case of lightest ions (e.g. H^+, H_2^+ etc.). Especially when coated emitters are used, the ion current may cause lifetime issues of the gauge. We therefore recommend reducing the emission current at higher pressures.

5.2.12. Influence of magnetic fields

The simulations included assessment on the influence of external magnetic fields (Fig. 32) on the electron transmission and ion collection under the operation of the gauge with different electron emitters (tungsten wire, disk 0.84 mm and disk 1.2 mm). A field of 50 μT already affects the electron trajectories, although all electrons still end up in the Faraday cup. Increase of the field to 100 μT leads to a huge disturbance of the trajectories and even the loss of many electrons. Finally, at 200 μT not a single electron reaches the Faraday cup. For comparison, the maximum Earth magnetic field on the Earth's surface is in the range of 25 μT–65 μT. Because of this rather strong sensitivity to magnetic stray fields, we recommend using a magnetic shielding with Mu-metal.

5.2.13. Tungsten wire as an emitter

As mentioned earlier, we aimed at commercially available emitters to make the gauge easy to manufacture. However, it would be preferable not to depend on a specific emitting cathode for a generic recommendation for an ion gauge reference standard. Therefore, we also investigated the use of U-shaped tungsten filaments (Fig. 33), which can be easily produced from a tungsten wire. By modifying the Wehnelt and ionisation cage entry, we achieved similar performance and misalignment tolerances as with the disk emitter. The length of the emitting section of the filament (of diameter d = 0.1 mm), i.e. the part parallel to the entry plane, is chosen such that the emitting area is approximately the same as for the disk emitter.

6. First measurements

Gauges of the designed and simulated type have been manufactured. Measurements indicate that, in terms of electron and ion trajectories, the gauges behave as expected by the simulations.

Measurements on the first gauges show sensitivities for nitrogen between 0.287 Pa^{-1} and 0.293 Pa^{-1} (Table 5). The simulated sensitivity for Argon results in $S_{Ar} = 0.320$ Pa^{-1} (OPERA) at nominal settings and taking into account the energy dependence of the ionisation cross-section in Fig. 1. This corresponds to a relative sensitivity of $S_{Ar}/S_{N2} = 1.11$, which is in good agreement with the measurements. Comparing the cross-sections only at the nominal electron energy of 200 eV results in $S_{Ar}/S_{N2} = 1.08$. The difference is caused by the potential dip close to the collector ring.

Fig. 34 shows the measured emission current and transmission efficiency as function of the Wehnelt potential obtained with Gauge 2 and compares with the simulation done with COMSOL. Above 35 V, the transmission starts decreasing in both simulations and measurements. The decrease is less pronounced in the simulation. As can be seen in Fig. 35, the difference is caused by the filament heating current, which

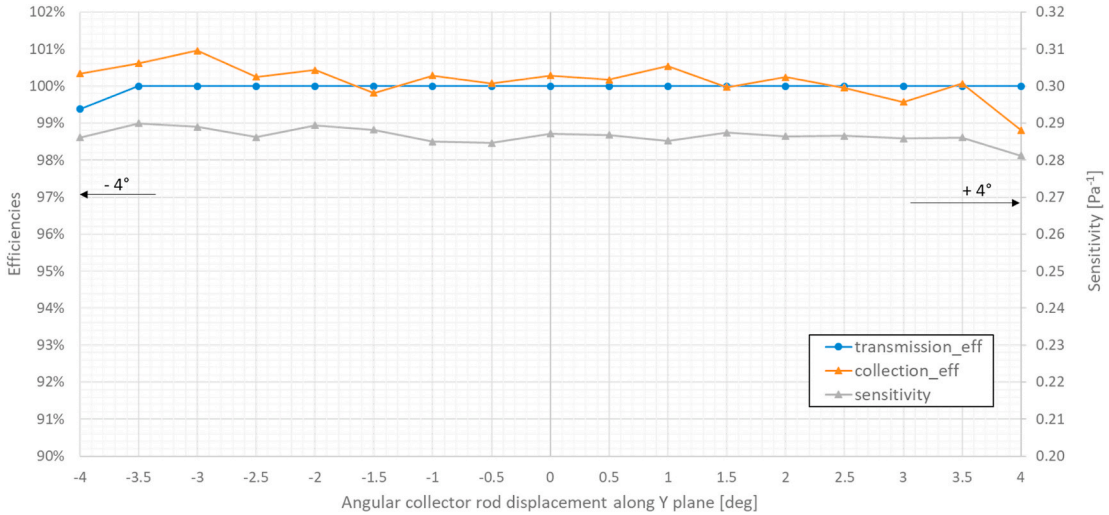

Fig. 30. Collector rod alignment along the Y-direction.

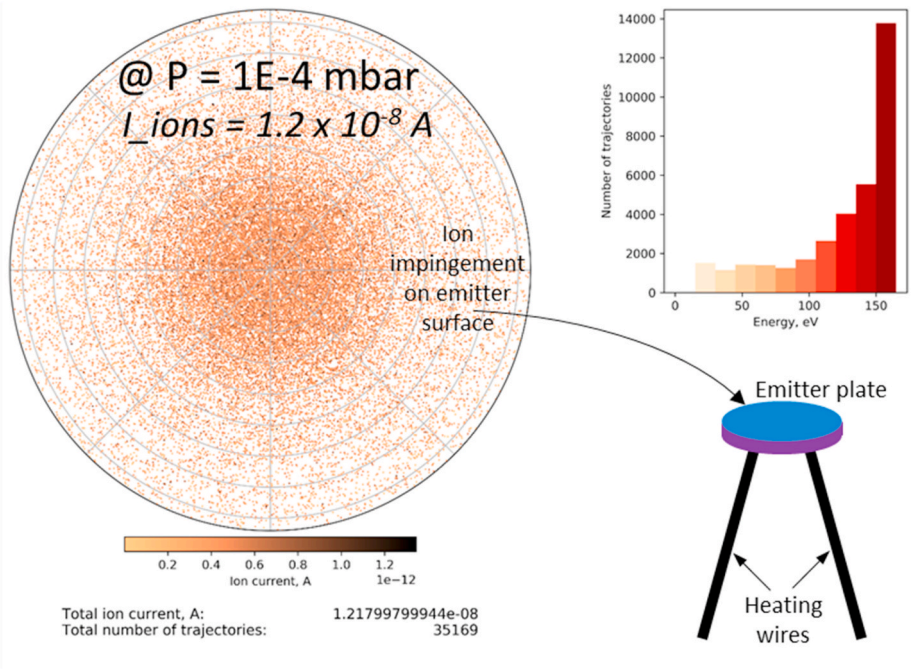

Fig. 31. Ion impingement on emitter disk. The emitter disk is spot-welded on the heating wire.

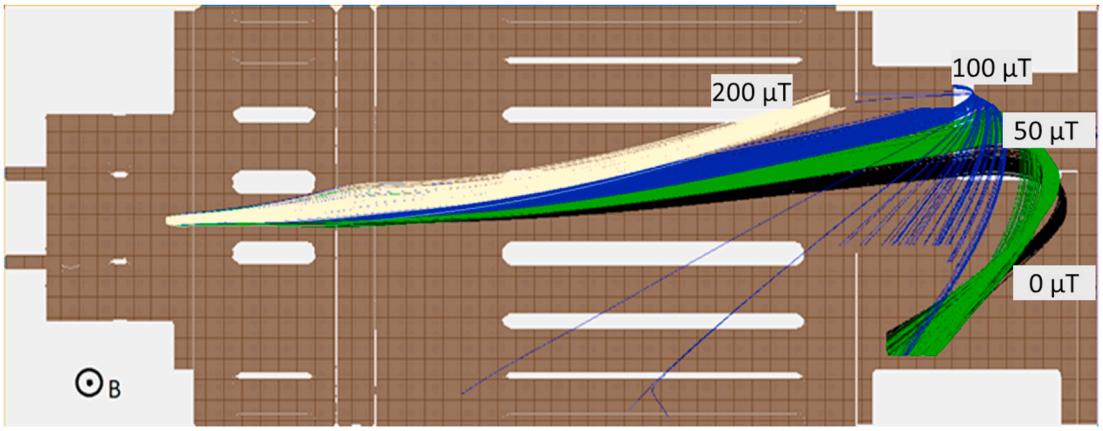

Fig. 32. Simulations of the electron trajectory (here with SIMION) in the presence of a magnetic field normal to the plane of the figure.

implies also higher emission currents at given Wehnelt potentials.

The optimal Wehnelt potential is the one, at which the emission current is maximal with the electron transmission efficiency still not affected. For the Gauge 2, shown here as example, that would be for a heating current of 1.447A at around 33 V.

One may notice that the flat top of the electron transmission efficiency is at 97% only, rather than at 100% as expected. This is also the case for Gauge 3. The missing percentage seems to be caused by reflected or high-energy secondary electrons from the Faraday cup. Most of these secondary electrons that contribute to the fictious reduced transmission end there trajectories on the small exit tube and do therefore not contribute to gas ionisation inside the ionisation volume. These electrons do not affect the sensitivity. Operating the gauge at higher Faraday cup potentials increased the transmission efficiency to above 99% whilst the sensitivity remained unchanged.

Gauge 1 has a different electron transmission behaviour (see Fig. 36). It does not show the expected flat top, but has two pronounced maxima. Simulations with COMSOL suggest that a strongly misaligned emitter causes this behaviour, but the gauge still performs rather well when operating at a Wehnelt potential of 34 V, as can be seen in Table 5.

The relative sensitivity factor for argon has been measured for Gauge 1 over a period of 10 days and remained constant within 0.57% (95% confidence interval). Figs. 37 and 38 show the repeatability and the linearity with pressure over this period.

Experimental evaluation of the gauge design will be presented in a separate article.

7. Conclusions and outlook

The software packages used for the simulations, SIMION, OPERA, and COMSOL proved to be valuable and helpful tools to design and evaluate new concepts of ionisation gauges. We found a promising new design of an ionisation vacuum gauge, that is suitable as a reference standard. It eliminates the broad variation of electron trajectories with poorly known values of the path length in the ionisation volume in Bayard-Alpert gauges. Instead, the electron trajectories, their path lengths and their energy in the ionisation volume are well known in our design and it was no surprise that the calculated, the simulated and the measured sensitivities for this new ionisation gauge type fully agree. A requirement for this result was that the ion collection efficiency is close

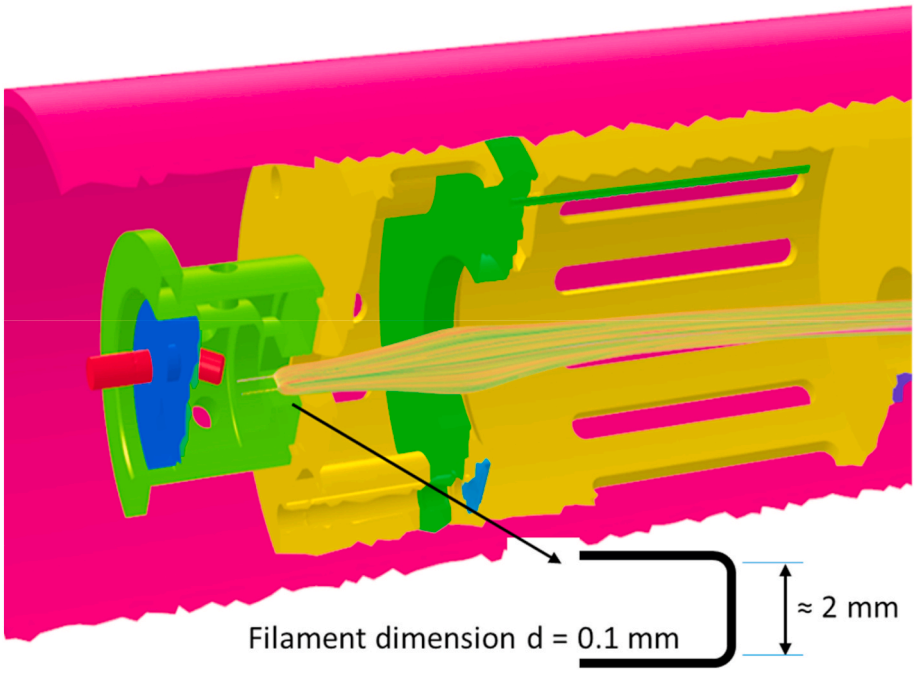

Fig. 33. Gauge with tungsten filament as emitter and modified optics at the entry of the ionisation volume.

Table 5
Sensitivities for nitrogen and argon measured on the first gauges and, for comparison, the values from the simulations.

	Gauge 1	Gauge 2	Gauge 3	Gauge 4	Simulation OPERA	Simulation SIMION	Simulation COMSOL
S_{N2} [Pa^{-1}]	0.293	0.290	0.287	0.291	0.288	0.297	0.281
S_{Ar} [Pa^{-1}]	0.328	0.328	0.322	0.327	0.320	–	–
S_{Ar}/S_{N2}	1.12	1.13	1.13	1.13	1.11	–	–

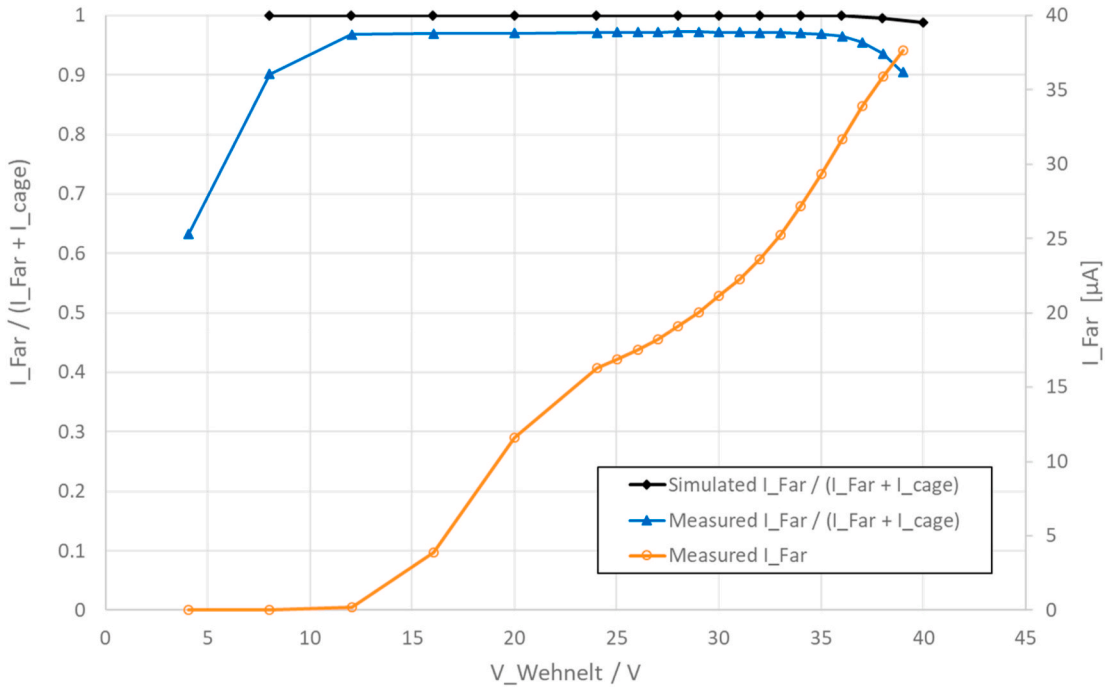

Fig. 34. Measured electron transmission efficiency and emission current of Gauge 2 at constant heater current at the emitter (1.447 A). The black line is the simulated electron transmission efficiency (COMSOL).

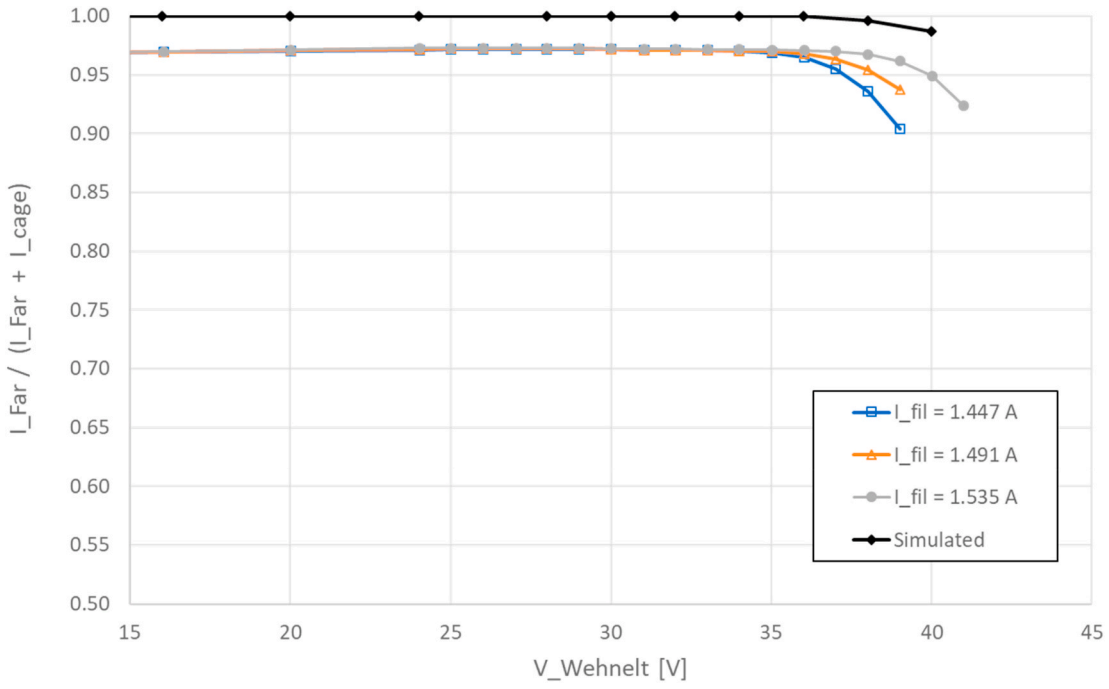

Fig. 35. Measured electron transmission (Gauge 2) at different filament heating currents as function of Wehnelt potentials.

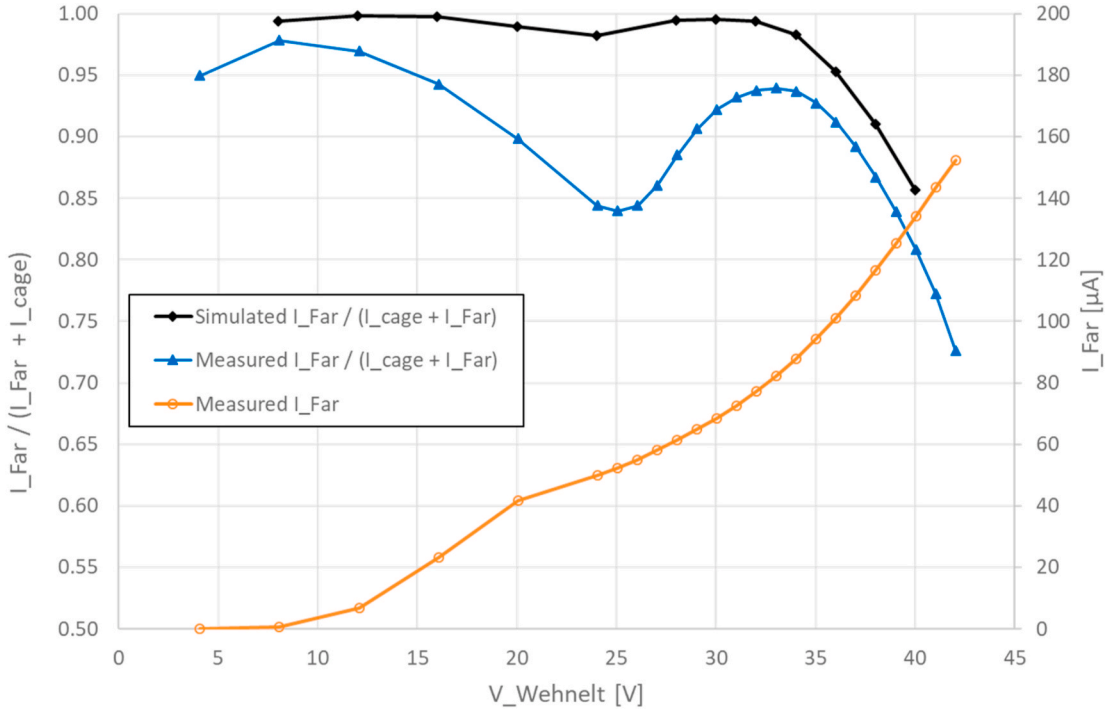

Fig. 36. Measured electron transmission and emission current for Gauge 1 compared with a simulation with a misaligned emitter (dY = 1 mm combined with a rotated disk of 30°).

to 100%. By this new gauge type it will be possible to ensure gauge independent relative gas sensitivity factors which are important to calibrate partial pressure analysers, determine pumping speeds or determine true pressures in industrial processes. It can be even expected that the relative gas sensitivity factors can be predicted from values of the ionisation cross sections by electrons so that no experimental determination will be necessary. Another interesting aspect of this design is the fact that many disturbances to the measurement and anomalies such as magnetic fields or electrode misalignments will affect the electron transmission. The electron transmission is measurable in this design. An unaffected electron transmission (close to 100%) is therefore an indicator that the measurements can be trusted with high confidence.

At present, manufactured gauges of this design are tested in our laboratories. Two different companies produced them with different layouts, but the sensitivities of the two layouts fully agreed. This

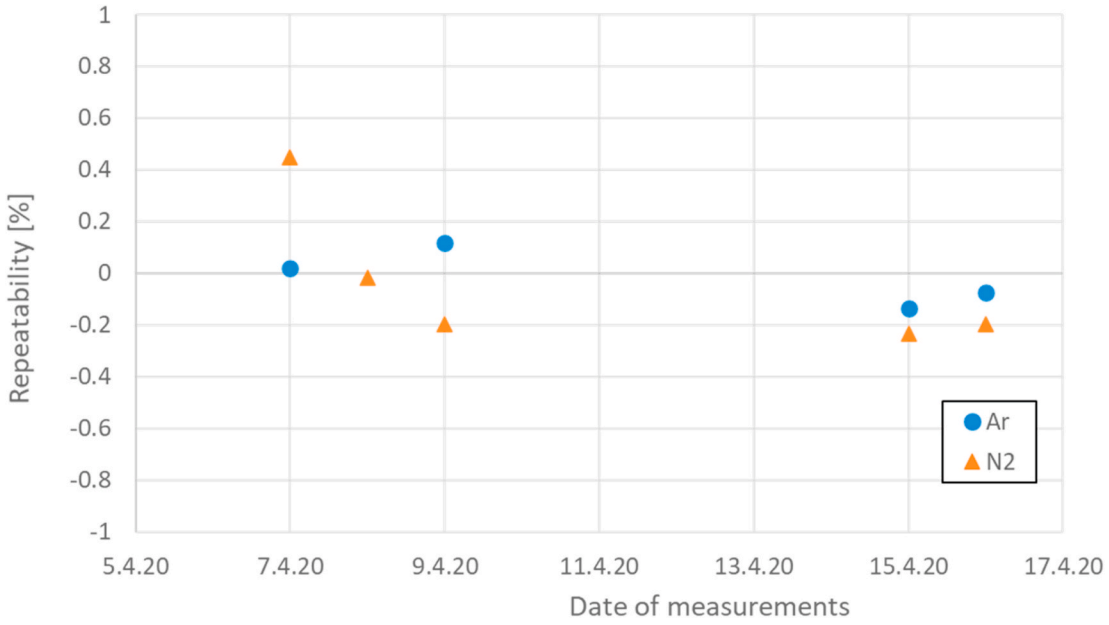

Fig. 37. Repeatability of the sensitivity for argon and nitrogen of Gauge 1 in Table 5.

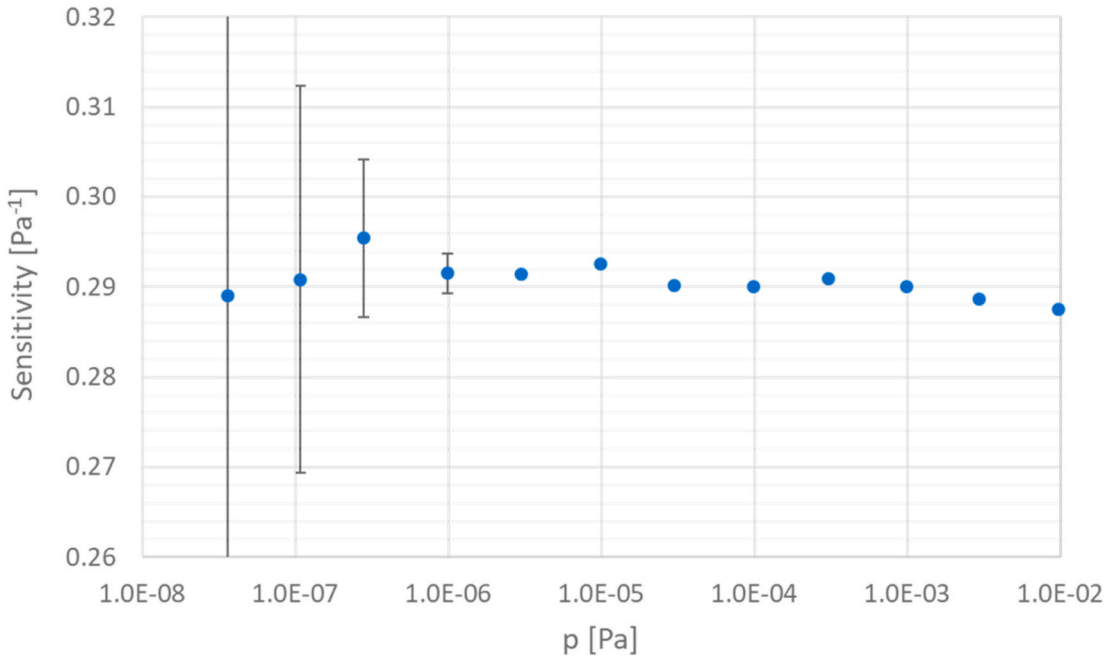

Fig. 38. Linearity with nitrogen pressure (Gauge 1). Measurements were taken at the fundamental measurement system for HV/UHV pressures CE3 of PTB [24]. The high uncertainties below 10^{-6} Pa are due to the uncertainties of current measurement.

indicates that the new gauge type can be produced with the same performance values independent of a manufacturer. Some technical problems were discovered which are not caused by the design, but by its realisation. Measurements on the transport stability, repeated calibrations with different gases after venting and cathode exchange, and long-term stability are ongoing. We will report on the evaluation of the produced gauges in another publication and propose to the ISO technical committee TC 112 to initiate a project for standardisation of this new ionisation vacuum gauge design. After the technical realisation of this gauge type has matured, we think that this gauge type will also be sufficiently robust to serve as a reference standard for calibration laboratories.

Declaration of competing interest

The authors declare that they have no known competing financial interests or personal relationships that could have appeared to influence the work reported in this paper.

Acknowledgement

This project has received funding from the EMPIR programme, co-financed by the Participating States and from the European Union's Horizon 2020 research and innovation programme, and the Portuguese National Funding Agency for Science, Research and Technology in the framework of the project UID/FIS/00068/2019.

References

[1] K. Jousten, et al., A review on hot cathode ionisation gauges with focus on a suitable design for measurement accuracy and stability, September 179, https://doi.org/10.1016/j.vacuum.2020.109545, 2020, 109545.

[2] P.C. Arnold, et al., Stable and reproducible Bayard-Alpert ionisation gauge, J. Vac. Sci. Technol. 12 (2) (Mar/Apr 1994) 580–586.

[3] D. Li, K. Jousten, Comparison of some metrological characteristics of hot and cold cathode ionisation gauges, Vacuum 70 (2003) 531–541.

[4] J.A. Fedchak, D.R. Defibaugh, Long-term stability of metal-envelope enclosed Bayard-Alpert ionisation gauges, J. Vac. Sci. Technol. 30 (6) (2012), 061601.

[5] 29.05.2020, https://physics.nist.gov/PhysRefData/Ionization/intro.html.

[6] Winifred Huo, Yong-Ki Kim, Use of relativistic effective core potentials in the calculation of total electron-impact ionization cross-sections, Chem. Phys. Lett. 319 (03 2000) 576–586.

[7] O.W. Richardson, The influence of gases on the emission of electrons and ions from hot metals, Proceedings of the Royal Society A, V91, Issue 633 (1915).

[8] 29.05.2020, https://en.wikipedia.org/wiki/Thermionic_emission#Richardson's_Law.

[9] I. Figueiredo, N. Bundaleski, O.M.N.D. Teodoro, K. Jousten, C. Illgen, Influence of Ion Induced Secondary Electron Emission on the Stability of Ionisation Gauges, submitted to Vacuum, 2020. https://doi.org/10.1016/j.vacuum.2020.109907.

[10] P. Costa Pinto, et al., Carbon coatings with low secondary electron yield, Vacuum 98 (December 2013) 29–36, https://doi.org/10.1016/j.vacuum.2013.03.001.

[11] R. Valizadeh, et al., Multipactor Suppression by Laser Ablation Surface Engineering for Space Applications, JACoW Publishing, 2019, https://doi.org/10.18429/JACoW-IPAC2019-TUPMP051. IPAC.

[12] F. Watanabe, Ion spectroscopy gauge: total pressure measurements down to 10^{-12} Pa with discrimination against electron-stimulated-desorption ions, J. Vac. Sci. Technol. 10 (1992) 3333, https://doi.org/10.1116/1.577821.

[13] K. Jousten, P. Röhl, Comparison of the sensitivities of ionization gauges to hydrogen and deuterium, Vacuum 46 (1995) 9–12.

[14] A. Tegerup, Simulation of a Bayard-Alpert ionization gauge with the PIC code Warp, Master thesis, http://kth.diva-portal.org/smash/get/diva2:1180808/FULLTEXT01.pdf.

[15] P. Juda, B. Jenninger, P. Chiggiato, T. Richard, 3D-simulation of ionisation gauges and comparison with measurements, Vacuum 138 (2017) 173–177.

[16] D.A. Dahl, SIMION for the personal computer in reflection, Int. J. Mass Spectrom., Volume 200, Issues 1–3, 25 December 2000, Pages 3-25.

[17] R. Silva, N. Bundaleski, A.L. Fonseca, O.M.N.D. Teodoro, 3D-Simulation of a Bayard Alpert ionisation gauge using SIMION program, Vacuum 164 (2019) 300–307.

[18] J.B. Le Poole, Electron guns, state of the art, Nucl. Instrum. Methods 187 (1981) 241–244.

[19] A. Klopfer, An Ionisation Gauge for Measurement of Ultra-high Vacua, Transact. Of the 8th Nat. Symp. of the AVS and 2nd Int. Congr, Pergamon, New York, 1962, p. 439.

[20] D.G. Bills, P.C. Arnold, S.L. Dodgen, C.B. Van Clev, New ionisation gauge geometries providing stable and reproducible sensitivities, J. Vac. Sci. Technol. 2 (2) (1984) 163–167.

[21] M. F. Diaz-Aguado et al., Experimental investigation of total photoemission yield from new satellite surface materials, J. Spacecraft Rockets, Volume 56 Issue 1.

[22] J.J. Scholtz, D. Dijkkamp, R.W.A. Schmitz, Secondary electron emission properties, Philips J. Res. 50 (1996) 375–389.

[23] Kimball Physics technical specification for tantalum disc cathodes thermionic emitters, 29.05.2020, www.kimballphysics.com/cathode-specs-ta.

[24] K. Jousten, H. Menzer, D. Wandrey, R. Niepraschk, New, fully automated, primary standard for generating vacuum pressures between 10-10 Pa and 3 x 10-2 Pa with respect to residual pressure, Metrologia 36 (1999) 493–497.